

NASA CR-72356  
GEST-2100

TOPICAL REPORT  
IRRADIATION OF  $UO_2$  FUEL CLAD  
WITH TUNGSTEN-25 W/O RHENIUM (U)

by

T. L. Gregory, R. F. Boyle and J. C. Danko

Prepared for  
NATIONAL AERONAUTICS AND SPACE ADMINISTRATION

December, 1967

CONTRACT NAS 3-2544

Technical Management  
NASA/Lewis Research Center  
Cleveland, Ohio  
Direct Energy Conversion Systems Branch  
J. F. Mondt

**GENERAL  ELECTRIC**

Nuclear Thermionic Power Operation  
Nuclear Systems Programs  
P. O. Box 846  
Pleasanton, California

N74-72670

Unclas  
33388

00/99

(NASA-CR-72356) IRRADIATION OF  $UO_2$  FUEL  
CLAD WITH TUNGSTEN-25 W/O RHENIUM  
(General Electric Co.) 86 p

(CATEGORY)

(NASA CR OR TMX OR AD NUMBER)  
U. S. Government Agencies and

Contractors Only

### LEGAL NOTICE

This report was prepared as an account of Government sponsored work. Neither the United States, nor the National Aeronautics and Space Administration, nor any person acting on behalf of the National Aeronautics and Space Administration:

- A. Makes any warranty or representation, expressed or implied, with respect to the accuracy, completeness, or usefulness of the information contained in this report, or that the use of any information, apparatus, method, or process disclosed in this report may not infringe privately owned rights; or
- B. Assumes any liabilities with respect to the use of, or for damages resulting from the use of any information, apparatus, method, or process disclosed in this report.

As used in the above, "person acting on behalf of the National Aeronautics and Space Administration" includes any employee or contractor of the National Aeronautics and Space Administration, or employee of such contractor, to the extent that such employee or contractor of the National Aeronautics and Space Administration, access to, any information pursuant to his employment or contract with the National Aeronautics and Space Administration, or his employment with such contractor.

Requests for copies of this report should be referred to:

National Aeronautics and Space Administration  
Office of Scientific and Technical Information  
Attention: AFSS-A  
Washington, D. C. 20546

68-5957

RESTRICTED DATA  
Atomic Energy Act of 1954

NASA CR-72356  
GEST-2100

TOPICAL REPORT

IRRADIATION OF  $UO_2$  FUEL CLAD  
WITH TUNGSTEN-25 W/O RHENIUM (U)

by

T. L. Gregory, R. F. Boyle and J. C. Danko

Prepared for  
NATIONAL AERONAUTICS AND SPACE ADMINISTRATION

December, 1967

CONTRACT NAS 3-2544

Technical Management  
NASA/Lewis Research Center  
Cleveland, Ohio  
Direct Energy Conversion Systems Branch  
J. F. Mondt

General Electric Company  
Nuclear Thermionic Power Operation  
Nuclear Systems Programs  
P. O. Box 846  
Pleasanton, California

# GEST-2100

## TABLE OF CONTENTS

	Page
ABSTRACT	
SUMMARY	1
INTRODUCTION	6
CAPSULE EXPERIMENT 64-01-R1	7
A. Capsule Design	7
B. Characterization of Capsule Materials	10
1. Characterization of UO <sub>2</sub> Fuel	10
2. Characterization of W-25 w/o Re Clad	12
3. Capsule Filler Gas Composition	15
4. Structural Material	17
5. Thermocouples	17
C. Capsule Fabrication	18
D. Out-of-Pile Testing	18
1. Thermocouple Calibration Test	18
E. Capsule Facilities	21
RESULTS AND DISCUSSION	27
A. Capsule Operation History	27
B. Capsule Diagnostic Analysis	28
C. Data Reduction of Experiment 64-01-R1	35
D. Post Irradiation Analysis	36
1. Analysis of Capsule Flux Wires	39
2. Visual Examination of Capsule	39
3. Gross $\gamma$ -Scan of Specimens	40
4. Multi-Channel (512) $\gamma$ Scans of Specimens	43
5. Neutron Radiographs of Specimens	43
6. Calibration of Stem Thermocouples	44
7. Capsule Gas Analysis	46
8. Examination and Dimensional Measurements of the Emitters	47

TABLE OF CONTENTS - Continued

	Page
9. Mass Balance of Fission Products and Uranium	51
10. Fission Product and Uranium Analysis	52
11. Burnup Analysis of $\text{UO}_2$ Fuel	54
12. Measurements of the O/U Ratio of the $\text{UO}_2$ Fuel	55
13. Electrical Resistivity Measurements of W-25 w/o Re Stem	56
14. Metallographic Examinations	57
a. Emitter of Specimen No. 2	58
b. Emitter of Specimen No. 3	64
E. Proposed Mechanism for Emitter Swelling	71
REFERENCES	76

## LIST OF FIGURES

Figure No.		Page
1	Irradiation Specimen	8
2	Emitter Fuel/Clad Capsule Assembly	9
3	Photomicrograph of 1.5% Enriched $\text{UO}_2$ Pellet	13
4	Microstructure of 1.5% Enriched $\text{UO}_2$ Pellet	13
5	Longitudinal Cross-Section of the W-25 w/o Tube Material	14
6	Microstructure of the W-25 w/o Re Tube Material Transverse Section	14
7a	Specimen Parts Prior to Assembly	19
7b	Radiographs of Capsule 1 and 2 Prior to Assembly in Capsule Shroud	19
8	Four Specimens Assembled in Capsule Arrangement	20
9	Completed Capsule	20
10	Drawing of Thermocouple Calibration Apparatus	22
11	Clad Temperature vs Stem Temperature	23
12	Drawings of the Capsule Positioner Equipment	25
13	THTB Node Structure Upper Stem Region	30
14	THTB Node Structure Lower Stem Region	31
15	THTB Node Structure Lower Can	32
16	Node Structure Used for TØSS Calculation PBR Experiment 64-01-R1	33
17	Stem Temperature per Reactor Cycle for Each Specimen	37
18	Gross $\gamma$ Scan of Specimen No. 2	41
19	Gross $\gamma$ Scan of Specimen No. 3	42
20	Neutron Radiographs of Specimens 2 and 3	45

# GEST-2100

## LIST OF FIGURES - Continued

Figure No.		Page
21	Photographs of W-25 w/o Re Emitters after Irradiation	49
22	Change in Outside Diameter of Emitters	50
23	Transverse and Longitudinal Sections of Emitter of Specimen No. 2	59
24	Montage of W-25 w/o Re Clad $\text{UO}_2$ Fuel of Transverse Section of Specimen No. 2	60
25	Second Phase in Grain Boundaries of W-25 w/o Re Clad Transverse Section, Emitter No. 2	62
26	Spherical Particles within Grain Boundary Phase of W-25 w/o Re Clad. Transverse Section, Emitter No. 2	62
27	Microstructure of End Cap Material of Specimen No. 2 Longitudinal Section	63
28	Vent Hole in Emitter of Specimen No. 2, Longitudinal Section	65
29	Specimen No. 3, Transverse and Longitudinal Sections of the Emitter	66
30	Montage of W-25 w/o Re Clad $\text{UO}_2$ Fuel of Transverse Section of Specimen No. 3	67
31	Second Phase in W-25 w/o Re Clad of Emitter No. 3 Transverse Section	69
32	Internal Phase Within the Second Phase in the W-25 w/o Re Clad. Emitter No. 3, Transverse Section	69
33	Vent Hole of Emitter No. 3, Longitudinal Section	70
34	Schematic Fuel Temperature Cycle	72

# GEST-2100

## LIST OF TABLES

Table No.		Page
I	Kr-85 Gas Vented	3
II	Maximum Dimensional Changes of Fuel Clad	3
III	UO <sub>2</sub> Fuel Burnup	4
IV	Capsule Irradiation Test Conditions	7
V	Isotopic Analysis of UO <sub>2</sub> Pellets	11
VI	Chemical and Spectrographic Analysis of UO <sub>2</sub> Pellets	11
VII	Chemical-Spectrographic Analysis of W-25 w/o Re Tubing	15
VIII	Typical Temperatures for Nodes of Figures 13, 14, 15 and 16	34
IX	Post-Irradiation Operations	38
X	Calculated Neutron Flux	39
XI	Kr-85 Gas Release	47
XII	Maximum Dimensional Changes in Emitters	48
XIII	Mass Balance of Fission Products and Uranium in Capsule #4	53
XIV	UO <sub>2</sub> Fuel Burnup Analysis	54
XV	O/U Ratio Measurements of UO <sub>2</sub> Fuel	55
XVI	Electrical Measurements of W-25 w/o Re Stem	57

GEST-2100

IRRADIATION OF  $\text{UO}_2$  FUEL CLAD  
WITH TUNGSTEN-25 W/O RHENIUM

ABSTRACT

A fueled irradiation capsule was designed, fabricated and tested in the NASA Plum Brook Reactor. The capsule consisted of four bulk uranium dioxide ( $\text{UO}_2$ ) fuel pellets clad with tungsten-25 weight percent (W-25 w/o Re). The clad end caps contained vent holes for the escape of fission gases. Companion specimens were located in an upper and lower axial position in the capsule. The temperature of the capsule was sensed by two thermocouples for each specimen which were placed in the specimen stem. Control of the experiment was based on a specimen clad temperature of  $1650^\circ\text{C}$  of the two lower specimens. The capsule was irradiated in an in-core position to a fuel burnup of  $2.16 \times 10^{20}$  fissions/cc on the highest power specimen.

IRRADIATION OF  $\text{UO}_2$  FUEL CLAD  
WITH TUNGSTEN-25 W/O RHENIUM

SUMMARY

An irradiation experiment was performed to determine the characteristics of bulk  $\text{UO}_2$  fuel specimens clad with tungsten-25 weight percent rhenium in a configuration representative of a nuclear thermionic converter for space power reactors. The specific objectives of the experiment were:

1. Achieve a fuel burnup greater than  $1 \times 10^{20}$  fissions/cm<sup>3</sup> with a clad temperature of 1650°C.
2. Measure the amount of fission gases that escapes through vent holes in the end cap.
3. Measure the quantity of  $\text{UO}_2$  that escapes through the vent holes.
4. Obtain information on the behavior of fission products.
5. Determine the structural integrity of the fuel/clad specimen.
6. Determine the  $\text{UO}_2$ -W-25 w/o Re compatibility in a nuclear environment.

The experiment capsule was designed to accommodate four irradiation specimens. The dimensions of each fueled emitter were 0.456-inch in diameter by 1.350-inches long with an emitter thickness of 0.20-inch. Three 0.020-inch vent holes were located in each end cap of the cylindrical cladding. The four specimens were positioned in pairs, each pair was mounted vertically in the capsule. The two upper specimens were designed

## GEST-2100

for fuel enriched to 2.4% while the two lower specimens were designed for fuel of 1.5% enrichment. These enrichments were calculated to obtain equal power in the specimens based on the vertical neutron flux gradient in the Plum Brook Reactor. The upper and lower specimen pairs were unknowingly switched during capsule assembly, which caused the lower specimen to operate at twice the power density of the upper specimens during the irradiation. The space between the fuel/clad and the containment can of each specimen was filled, at room temperature, with one atmosphere of 75% argon-25% helium gas to conduct the heat from the clad to the containment can and maintain the proper temperature drop. The temperature of each fueled specimen was determined by measuring the support stem temperature and then using a calibration curve which relates the stem temperature to the clad temperature. An out-of-pile calibration experiment and calculations of in-pile gamma heating were used to establish the calibration curve. The capsule position was varied during the irradiation to maintain the lower specimen clad temperature at 1650°C.

The capsule was installed in test location LD-11 of the Plum Brook Reactor. The operating data from the first cycle showed that the lower specimen temperatures were much higher than expected. Therefore, the capsule was moved to the LA-11 test location where the neutron flux was lower. In this location the lower specimens could be maintained at a calculated clad temperature of 1650°C during a normal reactor operating cycle. Analytical studies were performed to resolve the uncertainties in the clad temperature and thermal power of each specimen. The standard deviation of the 1650°C clad temperature was calculated to be 110°C and of the 350 watts thermal power was calculated to be 70 watts. The irradiation of the capsule was terminated after a total of 3340 hours at operating temperature.

# GEST-2100

The significant post-test examination operations and results are:

1. The stainless steel containers were punctured and gas samples were successfully collected from specimens 2, 3, and 4. The gas was analyzed by gamma counting to determine the quantity of Kr-85 in each sample. The results are presented in Table I along with the calculated quantity of Kr-85 produced based on actual burnup data.

Table I  
Kr-85 Gas Vented

<u>Specimen</u>	<u>Kr-85 Atoms in the Gas Sample</u>	<u>Kr-85 Atoms Produced by Fission</u>	<u>% Vented</u>
2	$3.61 \times 10^{17}$	$4.67 \times 10^{17}$	77.3
3	$8.87 \times 10^{17}$	$10.3 \times 10^{17}$	86.1
4	$8.43 \times 10^{17}$	$9.53 \times 10^{17}$	88.5

2. Dimensional measurements were made on each fuel clad and the maximum change in dimensions are presented in Table II.

Table II  
Maximum Dimensional Changes of Fuel Clad

<u>Specimen</u>	<u>Diametral Change (inch)</u>	<u>Length Change (inch)</u>
1	+0.024	-0.002
2	+0.013	-0.001
3	+0.050	+0.040
4	+0.046	+0.035

3. The burnup analyses of the  $\text{UO}_2$  fuel was done by measuring the quantity of Nd and heavy element fission products in the fuel. The results are presented in Table III.

Table III  
UO<sub>2</sub> Fuel Burnup

<u>Specimen</u>	<u>Fissions/cm<sup>3</sup> Based on</u>	
	<u>Nd Measurements</u>	<u>Heavy Elements</u>
2	0.94	0.92
3	2.07	2.16
4	1.92	1.92

4. The quantity of UO<sub>2</sub> which escaped through the vent holes in specimen number 4 was determined to be 1.94 mgs which is less than 0.01 percent of fuel in one specimen. The vent holes in all specimens were completely open and only a trace of UO<sub>2</sub> was detected in the vent hole of specimen 3.
5. The UO<sub>2</sub>-W 25 w/o Re interface was completely separated with no evidence of bonding and no chemical interactions. The cladding was expanded but there were no cracks in the clad material.

A thorough examination of the post-test data and operational history indicates that the clad deformation resulted from thermal-mechanical interaction between the UO<sub>2</sub> fuel and the cladding. The proposed mechanism is described as follows:

1. The UO<sub>2</sub> fuel redeposits during the first few reactor cycles, such that the fuel and clad are in intimate contact at a given power density and temperature.
2. Then if the specimen is operated at a lower power density, the temperature is reduced and a gap forms between the fuel and clad because of difference in coefficients of thermal expansion.

GEST-2100

3. The  $\text{UO}_2$  fuel would then redeposit and be in intimate contact with clad at a lower temperature than initially.
4. Then if the specimen power density is increased to bring the clad temperature up to the original temperature, the clad would be expanded because the  $\text{UO}_2$  thermal expansion is greater than the W-Re clad.
5. Each succeeding power density change of this type which results in a major temperature change ( $200^\circ\text{C}$ ) would incrementally expand the clad.
6. The overall increase in clad dimensions would then be determined by the number of major temperature changes made during the operating life of the specimens.

## INTRODUCTION

In the design and development of high temperature thermionic fuel elements, an important consideration is the selection of the nuclear fuel and clad material. The properties of these materials in relation to their application must be evaluated along with their high temperature compatibility.

In previous work<sup>(1)</sup> under this technology program, the high temperature compatibility between a tungsten-25 weight percent rhenium (W-25 w/o Re) clad and uranium dioxide ( $\text{UO}_2$ ) nuclear fuel was demonstrated in out-of-pile tests. Therefore, an experiment was initiated to determine the high temperature irradiation characteristics of bulk  $\text{UO}_2$  clad with W-25 w/o Re.

The objectives of this irradiation experiment, Plum Brook Reactor No. 64-01-R1, were:

1. Irradiate to a  $1 \times 10^{20}$  fission/cc of fuel burnup.
2. Measure the fission gas release from bulk  $\text{UO}_2$  through peripheral vents in the W-25 w/o Re clad.
3. Measure the  $\text{UO}_2$  fuel loss through the vents.
4. Obtain information on the disposition of fission products.
5. Obtain information on the compatibility between the clad and fuel in a nuclear environment.
6. Determine the dimensional stability and structural integrity of bulk  $\text{UO}_2$  specimens clad with W-25 w/o Re material.

## CAPSULE EXPERIMENT 64-01-R1

## A. Capsule Design

The capsule design provided for testing four W-25 w/o Re clad bulk  $\text{UO}_2$  fueled specimens in Plum Brook Reactor under the test conditions shown in Table IV.

The necessary nuclear, heat transfer and mechanical design calculations were performed in the design of the experiment to meet the conditions listed in Table IV. Further, the dimensions of the clad-fuel specimens were to be representative of a high temperature fuel element that has application in nuclear thermionics.

Table IV  
Capsule Irradiation Test Conditions

Clad Temperature	$1650 \pm 221^\circ\text{C}$ ( $2\sigma$ )
Clad Specimen Environment	75% Argon-25% Helium
Thermal Flux	$0.3$ to $5 \times 10^{14}$ nv at 60 MW
Gamma Heat	$0.5$ to $7$ W/gm
Fuel Burnup	to $1 \times 10^{20}$ fissions/cc
Total Power	535 Watts
Fission Power	350 Watts $\pm 41\%$ ( $2\sigma$ )
Test Position	LA-11

The clad-fuel specimen configuration is illustrated in Figure 1. Four of these specimens were assembled into the irradiation capsule with the specimens mounted in pairs. Each pair was mounted side by side in a vertical position in the capsule as illustrated in Figure 2. The W-25 w/o Re clad contained three 0.020-inch diameter vent holes,  $120^\circ$  apart in the stem end cap. These vent holes were designed to provide escape passages for the fission gases. To achieve the desired operating conditions, the  $\text{UO}_2$

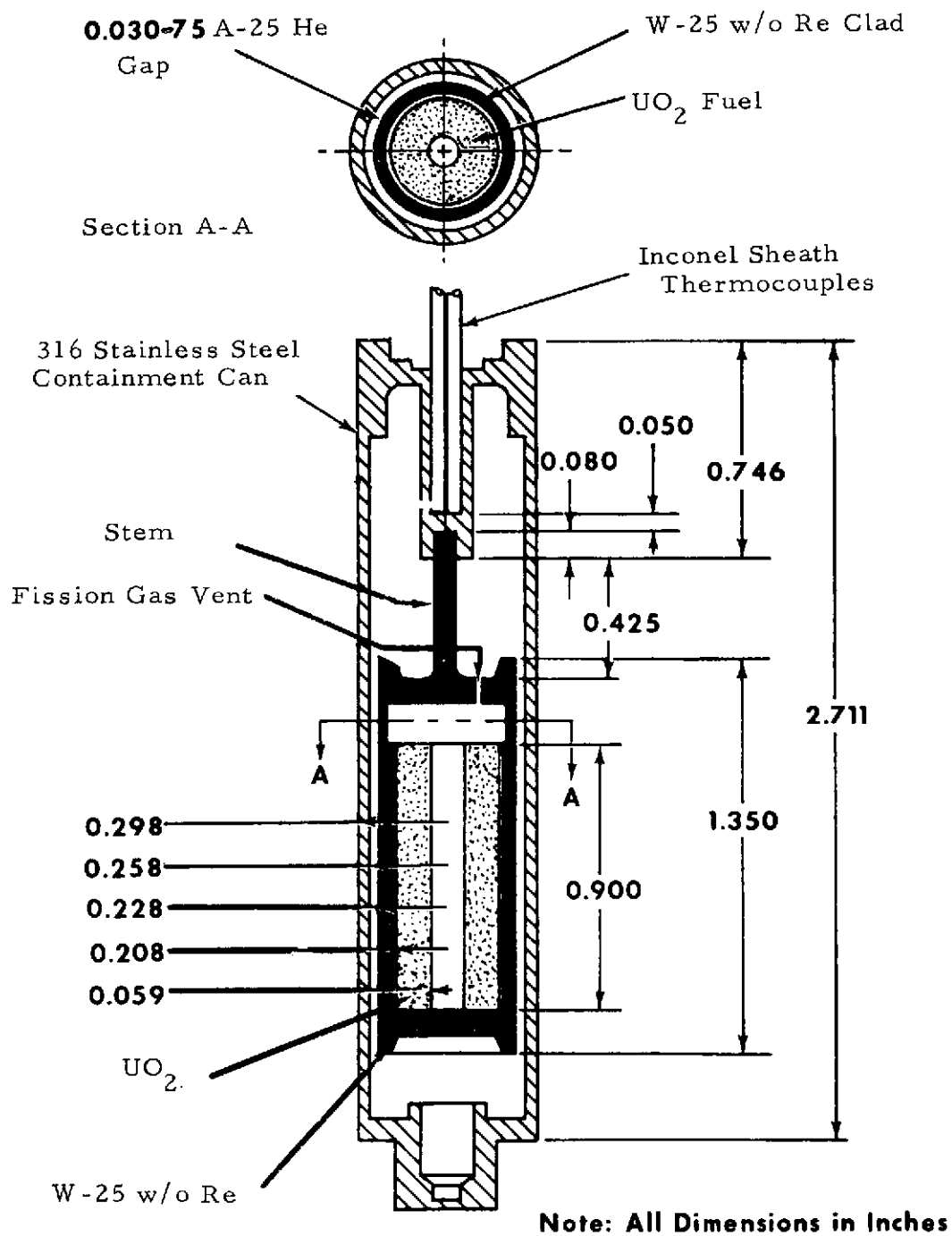


**FIGURE 1.** Figure 1. IRRADIATION SPECIMEN

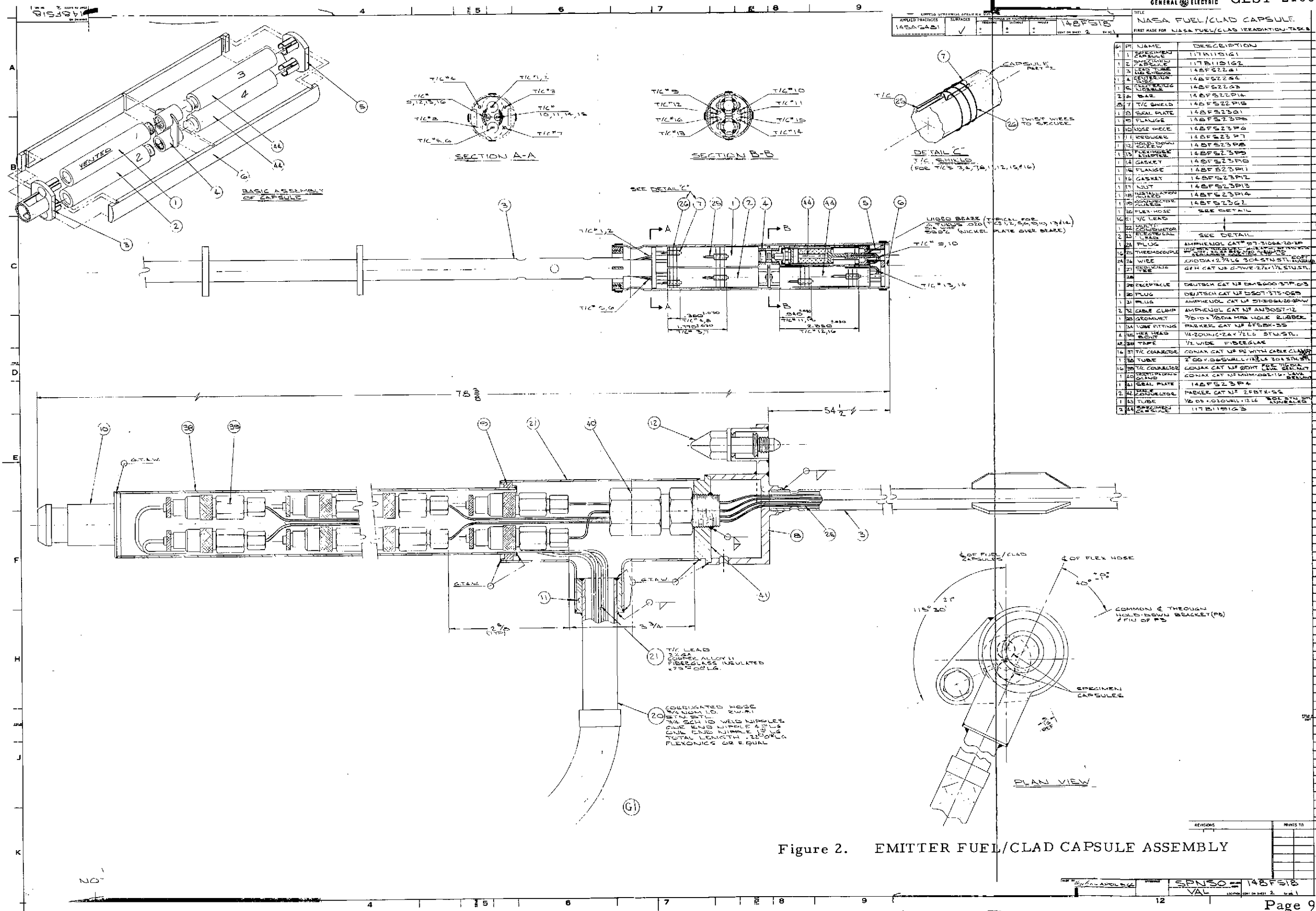


Figure 2. EMITTER FUEL/CLAD CAPSULE ASSEMBLY

fuel enrichment was designed to be 1.5% for the two lower specimens and 2.4% for the two upper specimens. The enrichments were determined by matching the fission power of the upper and lower specimens which is dependent on specimen location in the neutron flux.

## B. Characterization of Capsule Materials

### 1. Characterization of $\text{UO}_2$ Fuel

The cylindrical fuel pellets (0.402-inch od, 0.450-inch long with a 0.119-inch diameter center core) were fabricated by cold pressing the  $\text{UO}_2$  powder and sintering the pellets. To produce the desired enrichment, natural and 19.9% enriched  $\text{UO}_2$  powders were blended with a liquid (water) vehicle to provide 200 gram batches of the desired 1.50 and 2.40% enrichments.

The pellets were formed by cold pressing the powders at 20,000 psi. Water was used as a binder and no organic binders or lubricants were employed. The pellets were sintered for six hours at 1700-1750°C in hydrogen. The outside diameter was finished by centerless grinding and the core was removed by ultrasonic drilling. Finally, the pellets were cleaned and fired at 1200°C for four hours.

Samples of the finished pellets were analyzed and the isotopic analysis of one pellet from each batch is reported in Table V.

Table V  
Isotopic Analysis of UO<sub>2</sub> Pellets

Sample	Isotope	Atom %
1 (Nominal 1.5% Enrichment)	U-234	0.005 ± 0.0001
	235	1.55 ± 0.01
	236	0.010 ± 0.001
	238	98.44 ± 0.10
2 (Nominal 2.4% Enrichment)	U-234	0.160 ± 0.001
	235	2.47 ± 0.02
	236	0.010 ± 0.001
	238	97.36 ± 0.10

The chemical and spectrographic analysis and other pertinent data of one pellet from each batch is presented in Table VI.

Table VI  
Chemical and Spectrographic Analysis of UO<sub>2</sub> Pellets

Element	Enrichment	
	1.55%	2.47%
	ppm	
Ag	< 0.1	< 0.1
Al	54	54
B	< 0.2	< 0.2
Cd	< 1	< 1
C	15.7	17.3
Cr	8	10
Co	< 2	< 2
Cu	< 1	< 1
F	2.3	1.8
Fe	60	80
Mg	1	1
Mn	0.5	< 0.5
Mo	3	3
Ni	24	24
N	<10	50
Pb	< 1	< 1
Si	34	34
Sn	< 1	< 1
V	<15	<15
O/U Ratio	2.012	2.010
Pellet Density (%T. D.)	95.5	95.2
Weight (gms)-Specimen(1)	17.70	(3) 17.73
(2)	17.68	(4) 17.72

Metallographic analysis was performed on one pellet of each enrichment. Fine spherical metallic particles randomly distributed in the  $\text{UO}_2$  matrix were observed at high magnifications in both pellets and are shown in a photomicrograph of the 1.5% enriched pellet, Figure 3. These metallic particles are likely the metallic impurities or iron and nickel or an alloy of these two elements. The source of these trace impurities was probably contamination from Inconel containment vessels employed in the preparation of the  $\text{UO}_2$  powders. In the etched condition, Figure 4, the  $\text{UO}_2$  of both enrichments revealed a very fine grain size which is typical of  $\text{UO}_2$  sintered at 1700-1750°C. The photomicrographs of the 1.5% enriched  $\text{UO}_2$  pellet are also representative of the 2.4% enriched pellet.

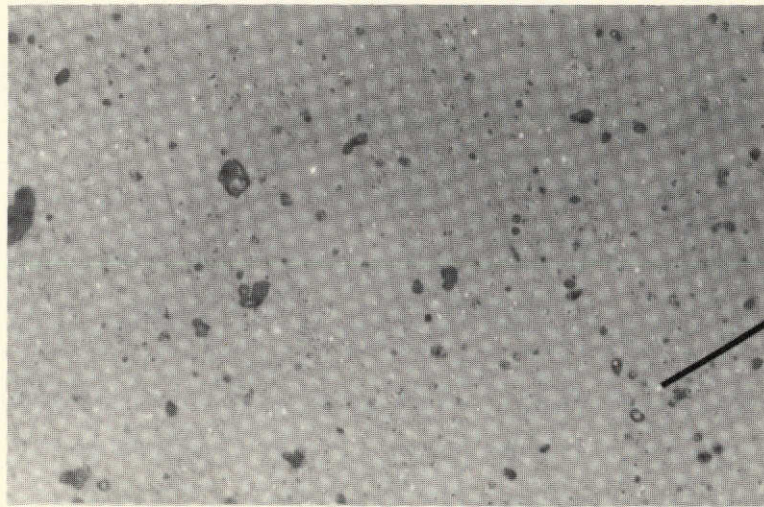
## 2. Characterization of W-25 w/o Re Clad

All of the tube and bar stock was produced by powder metallurgy techniques and were procured from Hoskins. Two W-25 w/o Re rods were produced; one was used for the preparation of the tubes and the bottom end caps while the other was used for the upper end cap-stem member. Both eloxing and grinding were used for the final machining of the parts. The results of the chemical analysis, spectrographic analysis and microhardness measurements of the as-received material are presented in Table VII. The chemical and spectrographic analysis of the upper end cap-stem material was very similar to that of the tube material except for 25 w/o Re, 81 ppm carbon and 220 ppm oxygen.

Metallographic examination of the W-25 w/o Re material was performed. No sigma phase was evident in either the tube or the upper end cap-stem material. In the longitudinal sections of the tube and end cap-stem material, the grains were elongated in the direction of working and the grain size was very similar. The transverse sections of these materials revealed an equiaxed fine grain structure. The microstructures of the longitudinal and transverse sections of the tube material are illustrated in Figure 5 and 6 respectively. These microstructures are also representative of the longitudinal and transverse sections of the upper end cap-stem material.

GEST-2100

(GENT-103)



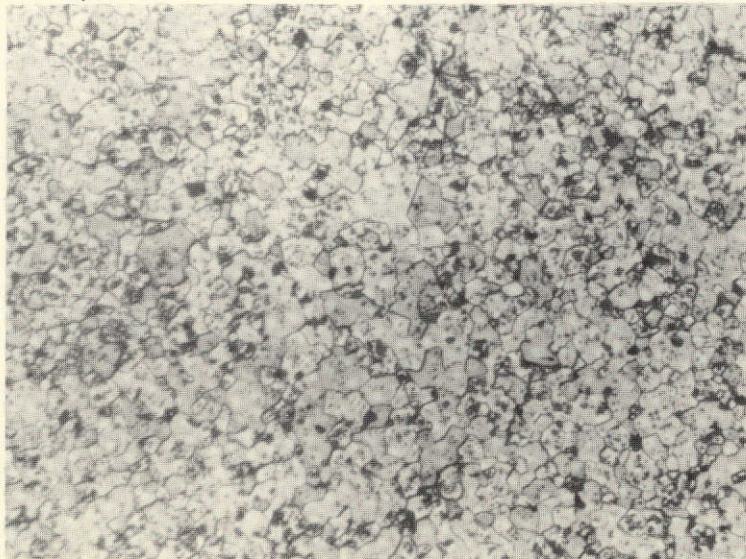
Metallic  
Particle

Unetched

1000X

Figure 3. PHOTOMICROGRAPH OF 1.5% ENRICHED  $\text{UO}_2$  PELLET

(GENT-104)



Etched

250X

Figure 4. MICROSTRUCTURE OF 1.5% ENRICHED  $\text{UO}_2$  PELLET

- GEST-2100

(GENT-105)

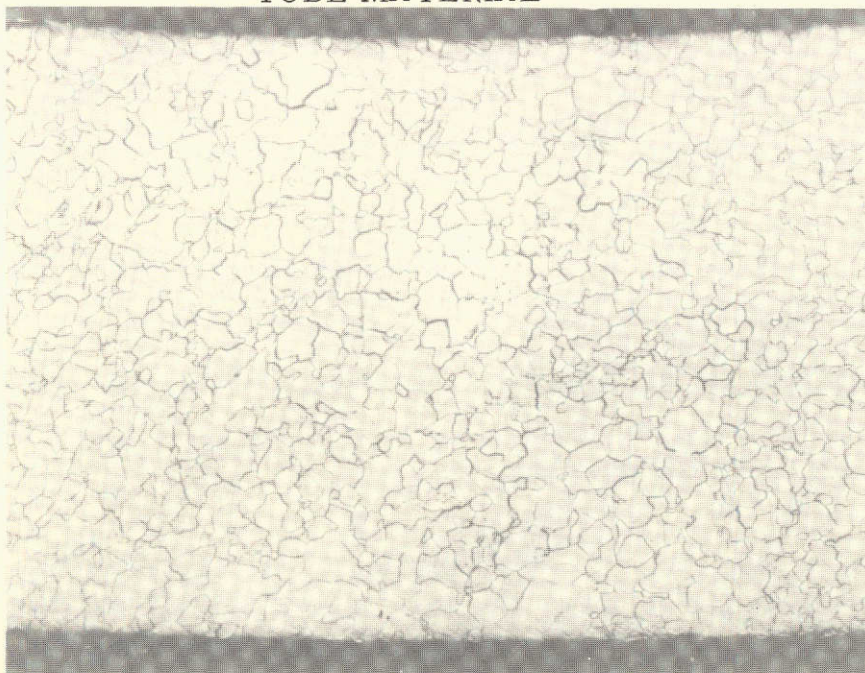


Etched

150X

Figure 5. LONGITUDINAL CROSS-SECTION OF THE W-25w/o Re TUBE MATERIAL

(GENT-106)



Etched

150X

Figure 6. MICROSTRUCTURE OF THE W-25 w/o Re TUBE MATERIAL TRANSVERSE SECTION

# GEST-2100

Table VII

## Chemical-Spectrographic Analysis of W-25 w/o Re Tubing

<u>Element</u>	<u>ppm</u>	<u>Element</u>	<u>ppm</u>
Ag	< 1	Mg	< 5
Al	<10	Mn	<10
B	<10	Mo	75
Ba	<10	Na	<10
Bi	<10	Ni	< 5
C	16	O	10
Ca	< 1	Pb	20
Cb	50	Sb	100
Co	< 5	Si	<10
Cr	<10	Sn	<10
Cu	2	Sr	<10
Fe	50	Ti	10
K	50	V	<10
		Zr	< 1

Re - 26.66 w/o

W - remainder

<u>Material</u>	<u>Microhardness</u> <u>DPH- 500 gm load</u>
Tube	440
Upper end cap-stem	446

The W-25 w/o Re material also passed a Zygo inspection for surface defects. A helium leak check was made on the tube stock and was helium leak tight to  $1 \times 10^{-8}$  cc/sec sensitivity.

### 3. Capsule Filler Gas Composition

On the basis of the capsule heat transfer analysis, an argon-helium gas mixture was selected to obtain the desired heat transfer across the gap between the fuel clad and stainless steel container. The composition and purity level of the gas were important to the success of the experiment, and therefore, an analysis of the gas was performed.

## GEST-2100

The gas was procured from Air Reduction Company ready-mixed in cylinders. The analysis of the as-received gas in the cylinder was:

Hydrogen	Not Detected
Helium	25.13 mole/o
Neon	Not Detected
Nitrogen	Not Detected
Oxygen	1.1 ppm
Argon	74.87 mole/o
Carbon Dioxide	0.25 ppm
Dew Point	-97°F

No other impurities were detectable with sensitivity threshold for impurities of 1.0 ppm.

The specimens were placed inside a vacuum glove box which was back filled with the gas mixture by 10 pump down and back filling cycles with approximately one hour soak at  $10\mu$  vacuum between cycles. The specimens were then welded shut at approximately 0.8 atmosphere. During the back filling and weld closure process, a sample bomb was in the box. At the time the closure weld was made, the bomb was sealed and the contents sent for analysis since it would be more representative of the specimen gas gap composition.

The bomb mass spectrometer analysis was as follows:

Hydrogen	0.10 mole/o
Water	0.03 mole/o
Nitrogen	0.35 mole/o
Oxygen	0.02 mole/o
Carbon Dioxide	0.01 mole/o
Neon	Not Detected
Helium	25.4 mole/o
Argon	74.1 mole/o

## GEST-2100

The level of accuracy for this analysis was:

0.01 mole/o	$\pm 20\%$
0.1 mole/o	$\pm 10\%$
1 and above	$\pm 2-3\%$

### 4. Structural Material

The containment can was fabricated from AISI Type-316 stainless steel. Since it served as a containment can for the fueled emitter in its cover gas with reactor cooling water on the outside, the material selection and stem design was in accordance with ASME Boiler and Pressure Vessel Code, Section III Nuclear Vessels. The material was certified per ASTM-SA276. The capsule support material was AISI Type-304 stainless steel while the shroud tube was made from 6061-T6 aluminum alloy. These materials are compatible with PBR reactor coolant system.

### 5. Thermocouples

Temperature measurements were made with two Pt vs Pt-13% Rh thermocouples positioned on each emitter stem of the four specimens. Two additional thermocouples were attached to the outside of each containment can of the four specimens to measure the water film temperature. Thus, a total of 16 thermocouples were used.

The Pt vs Pt-13% Rh thermocouples were sheathed in Inconel with a magnesium oxide (MgO) insulator. The nominal dimensions of the thermocouples were: outside sheath diameter - 0.062-inch, diameter of thermocouple wire - 0.012-inch. All of the thermocouples had grounded junctions and were helium leak tight to a sensitivity of  $1 \times 10^{-8}$  cc/sec as determined by a mass spectrometer. The junctions were non-destructively inspected for integrity and defects by a 100% radiographic examination. The thermocouples were calibrated by the vendor over the temperature range of 400 to 1000°F. A deviation of +0.2°F at the low temperature end and +0.67°F at

the high temperature end was observed.

### C. Capsule Fabrication

The parts that make up one of the four specimen assemblies and containment cans were prepared from the inspected and approved material. All four specimen parts ready for assembly are shown in Figure 7a. Two of the three 0.020-inch diameter vent holes in each clad end cap can be seen in the photograph. Also shown are the holes for the two thermocouples in the upper closure section. The final assembly of the specimens was performed using clean room procedures. The stainless steel containers were radiographed and leak tested after final weld closure and again after brazing in the stem thermocouples. Examination of the radiographs, see Figure 7b, indicated good alignment of parts and that the stems were intact on all specimens. Each container was helium leak checked on a mass spectrometer leak detector and no helium leakage was found.

The individual specimens were assembled into the capsule configuration shown in Figure 8. Two cobalt-aluminum flux wires were placed on the specimen to be used for post-irradiation evaluation of total thermal flux dose received during testing. The completed capsule with the aluminum cover in place is shown in Figure 9. The capsule was shipped to PBRF and pre-irradiation inspection and testing revealed that the capsule was ready for irradiation.

### D. Out-of-Pile Testing

#### 1. Thermocouple Calibration Test

An out-of-pile calibration test was performed to obtain the relation between the emitter surface temperature and the temperature sensed by the thermocouples located at the end of a tungsten rhenium support stem. The test consisted of a thermal mock-up of the clad and support stem as used in

GEST-2100

(GENT-107)

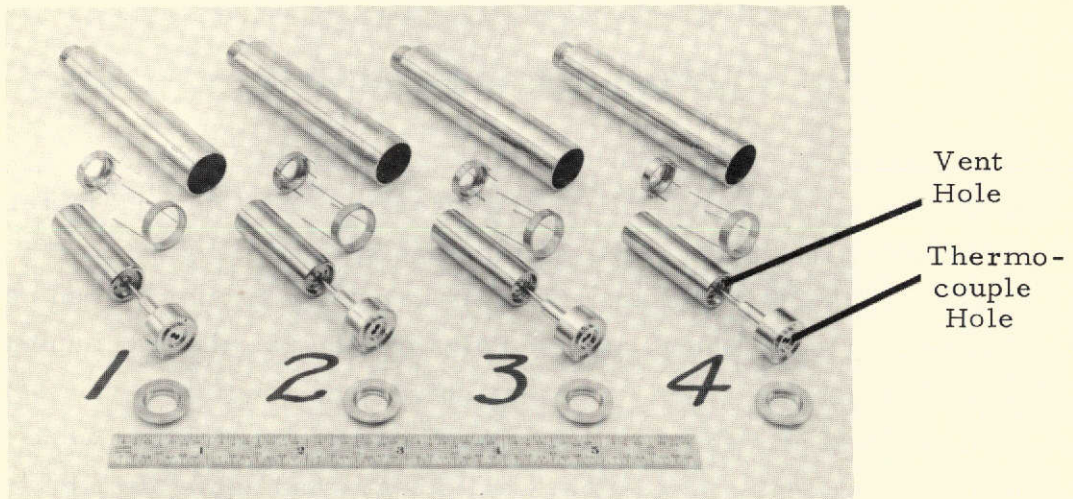


Figure 7a. SPECIMEN PARTS PRIOR TO ASSEMBLY

(GENT-108)

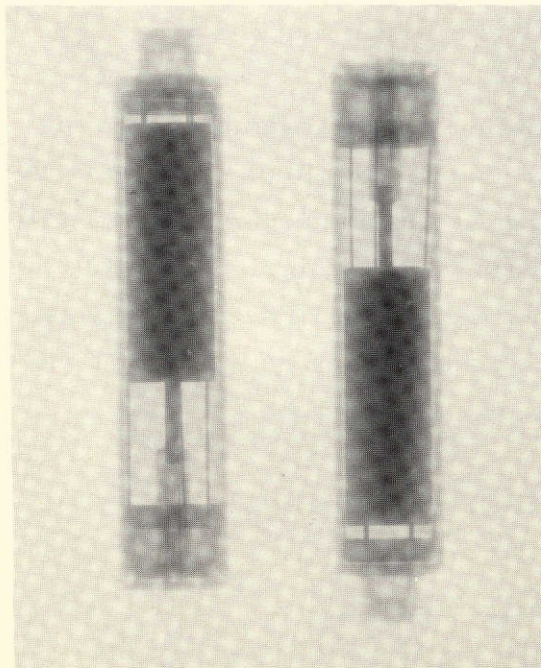


Figure 7b. RADIOGRAPHS OF CAPSULE 1 AND 2 PRIOR TO ASSEMBLY IN CAPSULE SHROUD

GEST-2100

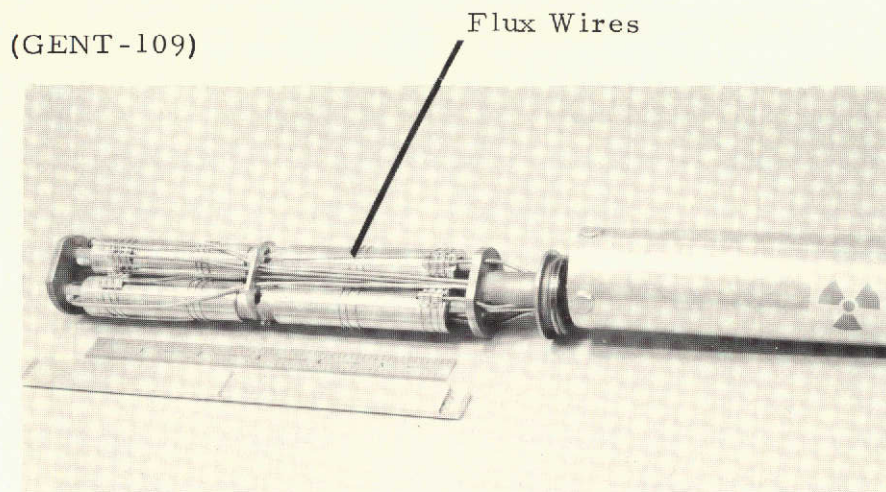


Figure 8. FOUR SPECIMENS ASSEMBLED IN CAPSULE  
ARRANGEMENT

(GENT-110)



Figure 9. COMPLETED CAPSULE

the irradiation specimen. This is shown in Figure 10. The cladding support stem, thermocouples, end cap, and water environment container were made of parts identical to those planned for the irradiation capsule. In the reactor experiment as in the calibration test, the specimen had two Inconel sheathed, Pt/Pt-13% Rh thermocouples brazed into the holes in the end of the support stem. In the out-of-pile test one thermocouple was tacked to the outside of the containment can and was used to measure the water temperature. A black body hole located in the W-25 w/o Re end cap was used for pyrometric temperature measurements. The four thermocouples were read out using a potentiometer and a suitable cold junction.

The results of the thermocouple calibration test are shown in Figure 11. The repeatability and agreement between thermocouples was within  $5^{\circ}\text{C}$ . The data indicated that at a clad temperature of  $1800^{\circ}\text{C}$ , the thermal conductivity of the W-25 w/o Re calculated for the observed temperature distribution ( $1350^{\circ}\text{C}$  average) was 0.63 watts/cm $^{\circ}\text{C}$ . This was approximately 5% lower than the value estimated using the Weidemann-Franz relation with a Lorenz number for tungsten and electrical conductivity data as a function of temperature for W-25 w/o Re. The calibration curve was used as the no gamma heat base curve for the final design calculations.

#### E. Capsule Facilities

In order to maintain a constant specimen temperature in the irradiation capsule, the experiment was provided with a positioner to move the capsule with respect to the PBR core. Thereby, the specimens could be moved during each reactor cycle with the neutron flux shift to maintain power generation, which in turn will establish the temperature.

This positioner, an electromechanical device, was designed to allow a maximum of ten inches of vertical movement with respect to the reactor core. The device penetrates the reactor pressure vessel and the position of the capsule was measured with respect to the core by using a position-

(GENT-111)

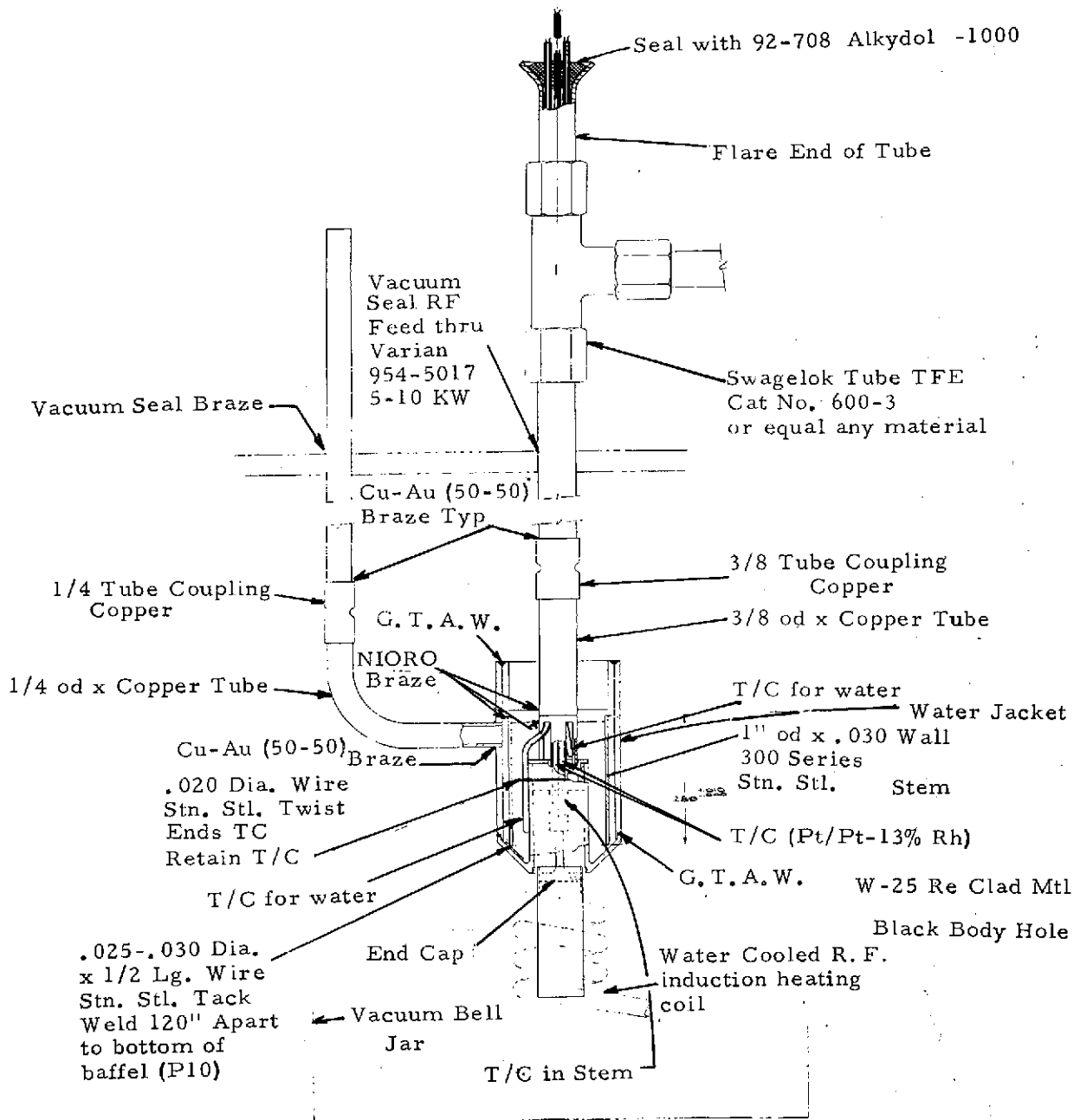


Figure 10. DRAWING OF THERMOCOUPLE CALIBRATION APPARATUS

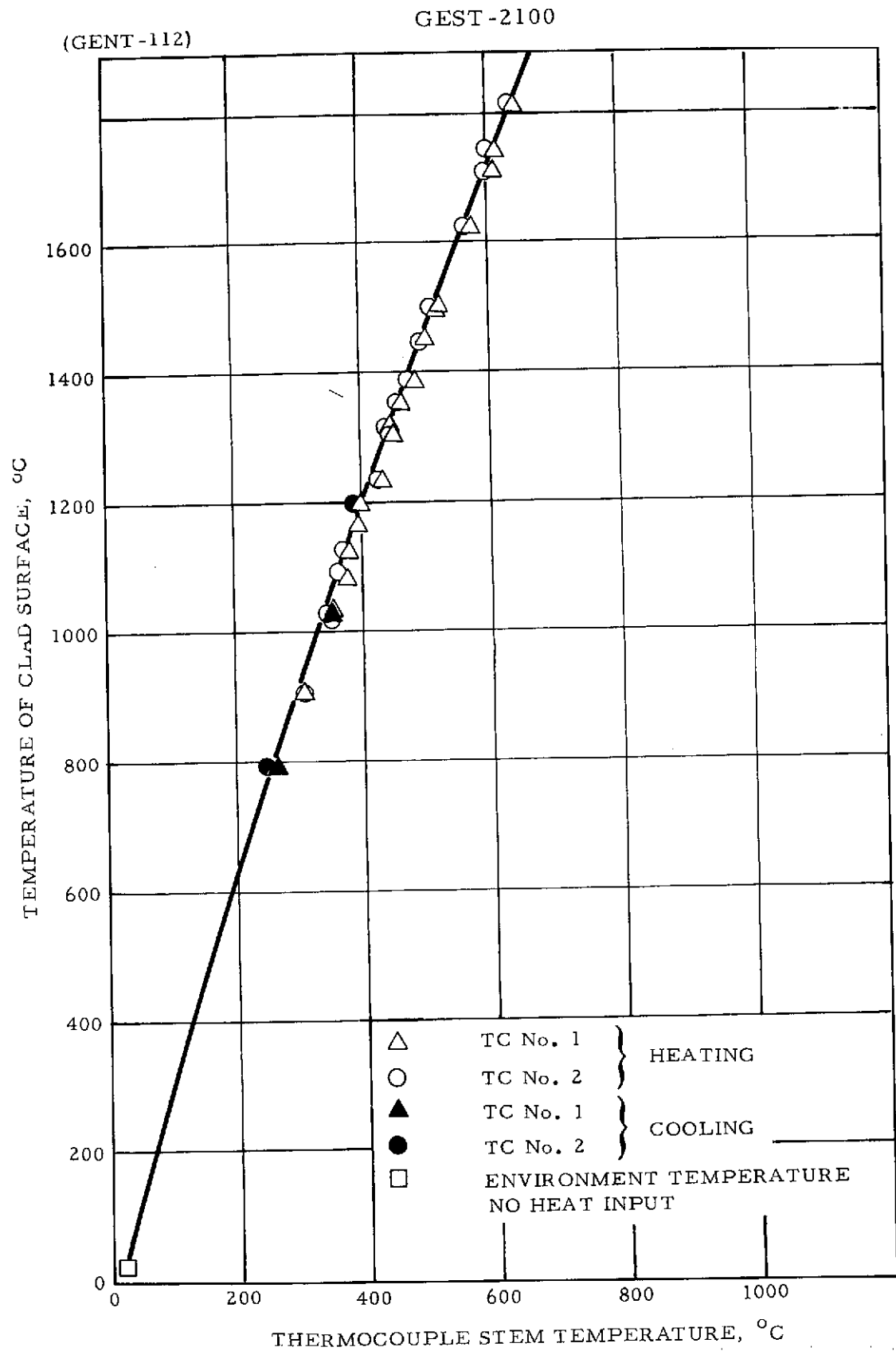


Figure 11. CLAD TEMPERATURE vs STEM TEMPERATURE

indicating transducer mounted outside the pressure vessel on a drive unit. The capsule positioner device was controlled from a console located outside the containment vessel.

The device consisted of four main assemblies: 1) an in-core facility tube, 2) a push-pull cable, 3) the pressure vessel seal, and 4) a drive unit. The capsule movement could be adjusted before installation to cover any 10-inch travel in the 24-inch vertical fuel region. The facility tube was designed with a capsule mounting plate on an actuating rod and to fit in a standard in-core PBR beryllium "L" piece spaced to provide a 0.075-inch cooling annulus. The downward flow of the coolant facilitated holding the tube in place; however, a suitable hold-down bracket was also provided. The vertical movement was achieved through the actuating rod mounted on linear ball bushings. The rod was attached to a ball-bearing, flex, push-pull cable.

The push-pull cable was routed up the inside wall of the reactor pressure vessel and was secured by instrumentation clamps. The external drive unit (Figure 12) consisted of a linear-motion pressure vessel seal attached to a flange designed to fit a 4-inch reactor vessel penetration. The seal consisted of a shaft through a double V-ring Teflon packing. The linear drive was powered by a reversible fractional horsepower (a-c phase shift) motor driving through a worm gear-screw-type mechanical actuator. The motor could be operated in either direction by using a circuit with a 3-position switch, for moving the capsule up or down from a remote console. The switch was a spring-loaded-type with center position off for operation safety. A linear-position transducer was mounted on an adjustable pad on the drive and was coupled to a key on the seal shaft. The transducer could be adjusted and calibrated to send a signal to a remote voltmeter calibrated to read in inches. The position of the capsule with respect to the reactor core could be measured to better than  $\pm 0.100$  inch.

(GENT-113)

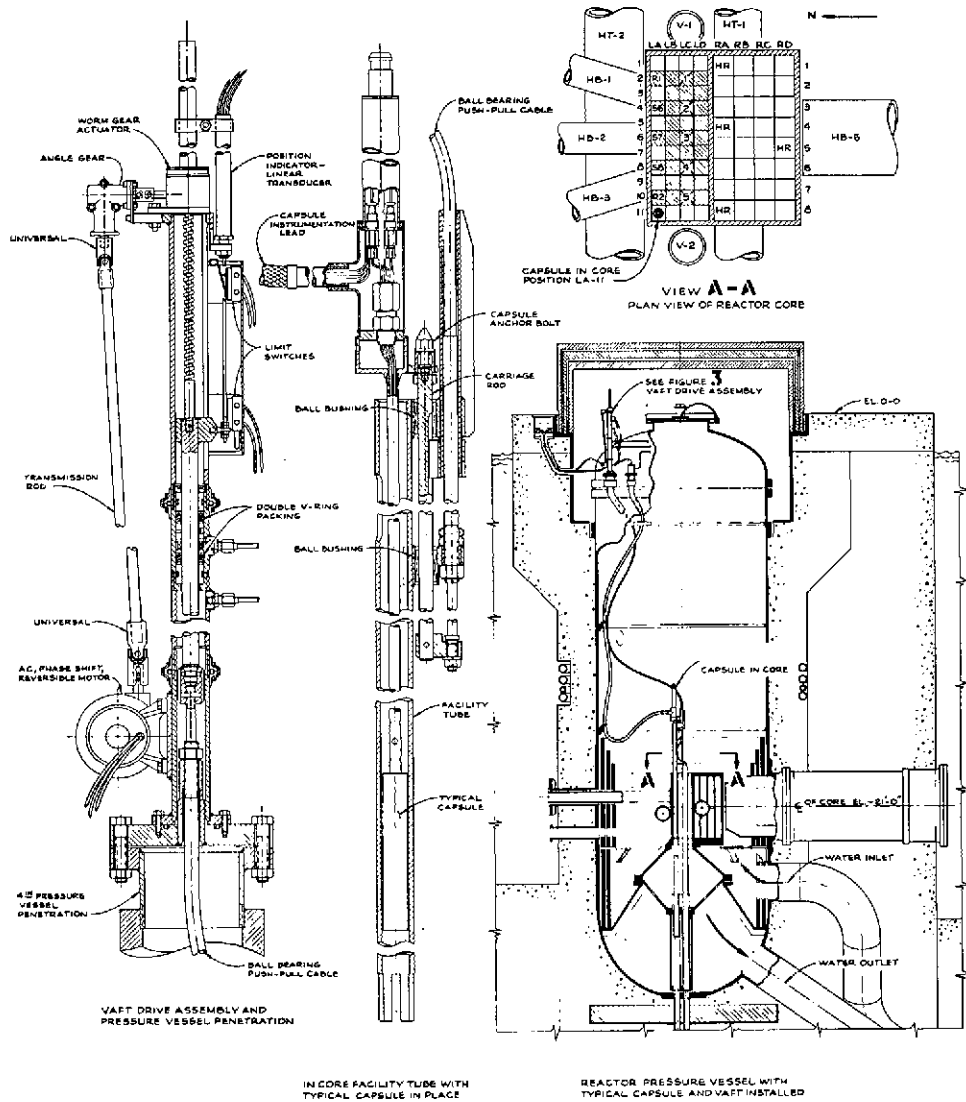


Figure 12. DRAWINGS OF THE CAPSULE POSITIONER EQUIPMENT

The seal for the linear-motion pressure vessel penetration was a double V-ring-type with a bleed between the packing layers. After the seal had been operated for several cycles under pressure, the leakage rate through the bleed port was less than 50 milliliters per day. The seal was designed for 150 psi and up to 150°F. However, the seal was tested to over 1.5 times the design pressure. Another bleed port was provided below the seal to allow venting of trapped air when the reactor vessel was pressurized.

A drawing of the capsule positioner equipment installed in the reactor vessel along with detailed drawings of the facility tube, vaft drive assembly and pressure vessel penetration seals are illustrated in Figure 12.

## RESULTS AND DISCUSSION

## A. Capsule Operation History

The irradiation of experiment 64-01-R1 started in PBR test position LD-11. During this reactor cycle, it was determined that as the reactor power was increased with the capsule in full-out position, more power was being generated in the fuel specimen than calculated. The power generation in the lower specimens was approximately a factor of 2 higher than expected for a given vertical position of the capsule and with the reactor operating at 50 MW only one inch insertion of the capsule would result in the desired temperature of the lower specimens. The upper specimens temperatures were significantly lower than expected. After 20-hours exposure, the upper specimens were a nominal  $900^{\circ}\text{C}$  and the lower specimens a nominal  $1700^{\circ}\text{C}$ , a difference of approximately  $800^{\circ}\text{C}$ . The predicted difference at startup was about  $300^{\circ}\text{C}$ . The lower specimens; i. e., 3 and 4, operated very close to the sample temperature as desired but the upper specimens, 1 and 2, were approximately  $100^{\circ}\text{C}$  apart in temperature.

Analysis of the data indicated that continued operation in LD-11 would result in specimen clad temperature higher than  $1800^{\circ}\text{C}$  with the capsule in the full-out position. Therefore, the reactor was shut down after 170 hours of operation and the capsule moved to position LA-11. A 2-1/8 inch spacer was placed under the VAFT in-pile tube in order to raise the specimens with respect to the core, thus operating in a lower flux region. With the lower flux in LA-11, elevating the test assembly with respect to the core and shadowing with the PBR regulation rod, the power generation in the capsule was reduced by a factor of approximately 2.

In LA-11 the lower specimens temperatures were at a nominal  $1650^{\circ}\text{C}$  and the upper specimen temperatures were at a nominal  $1250^{\circ}\text{C}$ , while the capsule was designed to operate at the same temperature. This temperature discrepancy could not be explained during the in-pile irradiation. However,

during post-test examination, it was discovered that the lower and upper specimens (different enrichment) had been switched prior to capsule assembly. Therefore, the 2.4% enriched specimens were the lower ones and the 1.5% enriched specimens were the upper ones, which explains the reason for the temperature difference between upper and lower specimens.

### B. Capsule Diagnostic Analysis

Additional analytical analysis was performed to resolve uncertainties in the temperature distribution and thermal power generation in the specimens. Analytical models were developed for reducing data from the experiment to temperature distribution and thermal power levels generated by fission, core gamma heating, and neutron induced gamma and beta heating. Included in the analysis were:

1. A perturbation analysis, performed with the DTF II multi-group neutron code, 14 non-thermal groups calculated by diffusion theory, and nine thermal groups calculated by transport theory.
2. An analytical description of the sources of heat generated in the capsule; i.e., core gamma heating, capture gamma and beta heating, and fission power.
3. A heat transfer analyses, performed with the THTB computer program (a finite difference analysis of three-dimensional transient heat flow). The following parameters were variables:
  - . Neutron flux
  - . Gamma heating
  - . Fuel enrichment
  - . Beta heating as a function of time
  - . Gas gap thermal conductivity
  - . Thermal conductivity of W/Re
  - . Thermal conductivity of stainless steel
  - . Total power
  - . Fission power
  - . Reactor water temperature

## GEST-2100

The base reference values were:

- . Neutron flux =  $1.202 \times 10^{14}$  nv
- . Gamma heating = 2.0 watts/gm (in  $H_2O$ )
- . Fuel enrichment = 1.5%
- . Total power = 536.1 watts
- . Reactor water temperature =  $120^\circ F$

The test specimens were divided into small nodal sections, Figures 13, 14 and 15, and the physical properties of each node were defined. Neighboring nodes were connected by specifying the common surfaces and formulations presented which defined the heat transfer interfaces between them. The resultant system of linear equations were solved by the Gauss-Siedel procedure. Iterations in time steps were conducted until the largest change in temperature between iteration for any node is within convergence criteria from 1.0 degree Fahrenheit for the first step to 0.01 degree for the two final steps. Using given values of coolant water temperature, sample cases were calculated to determine the temperatures of nodes. Regression analysis was employed to facilitate the reduction of multiple complex equations. Graphs were generated which show the relationship between thermocouple temperature, and between thermal power and mean cladding temperature and between neutron flux and mean cladding temperature. The uncertainties of temperature calculated by the method described were evaluated.

The temperatures for all the nodes shown in Figures 14, 15, and 16 are tabulated in Table VIII for a typical case. The values of the variable parameters for this case were:

- . Neutron flux =  $1.202 \times 10^{14}$  nv
  - . Gamma heating = 2.0 watts/gm (in  $H_2O$ )
  - . Fuel enrichment = 1.5% (lower specimens)
  - . Total power = 536.1 watts
  - . Reactor water temperature =  $120^\circ F$
  - . Beta heating for equilibrium core conditions
  - . Thermal conductivities of gas, W/Re and stainless steel for the original unirradiated case
  - . A convergence temperature tolerance of  $0.01^\circ F$
4. A comparative analysis was made between the TØSS computer program used for earlier calculations and the THTB computer program which these analyses are based upon. The TØSS program uses the first forward finite difference method and solves steady-state problems as the result of transient-type calculations. The nodal structure (Figure 16) employed in the TØSS program is less refined than was used for the THTB runs. Materials

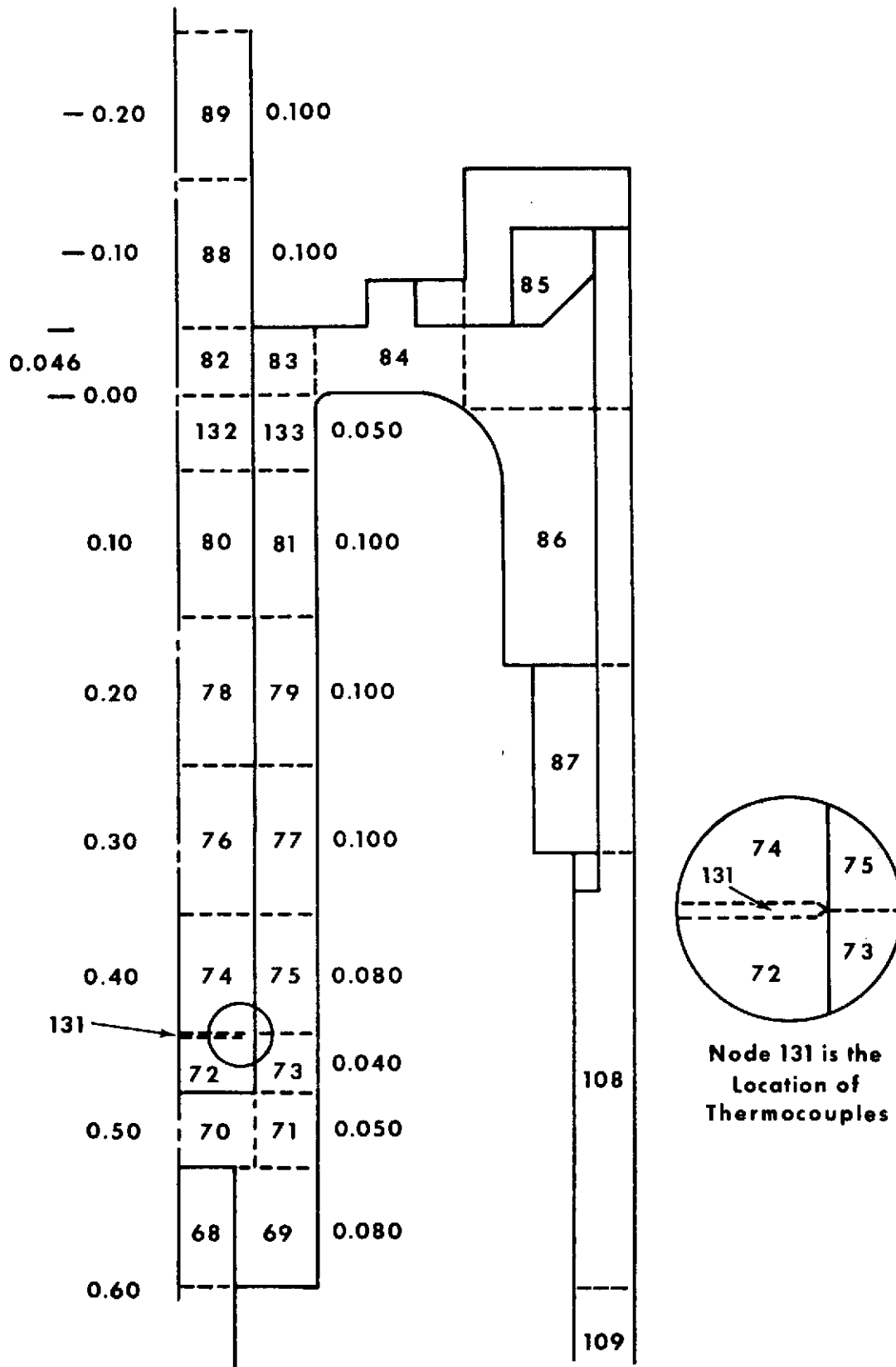


FIGURE 13. THTB NODE STRUCTURE UPPER STEM REGION

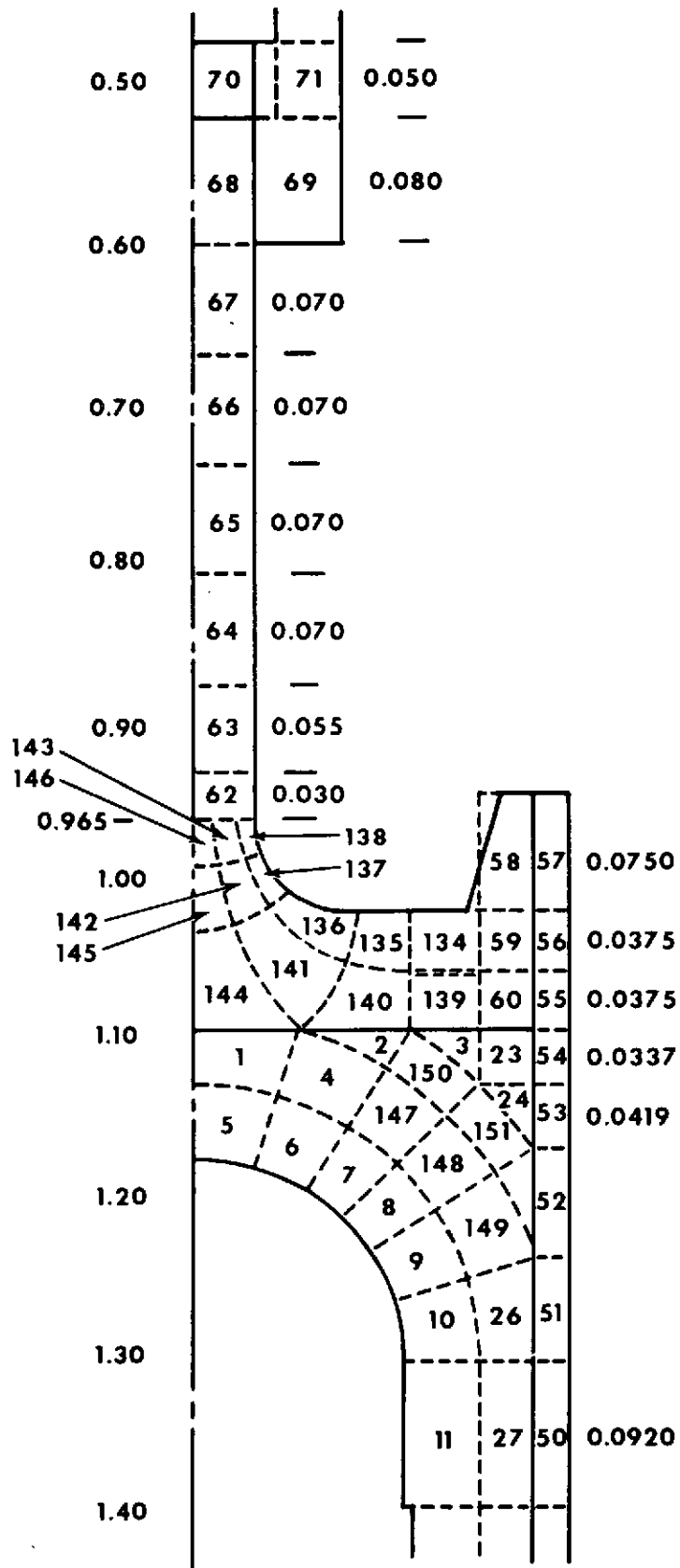
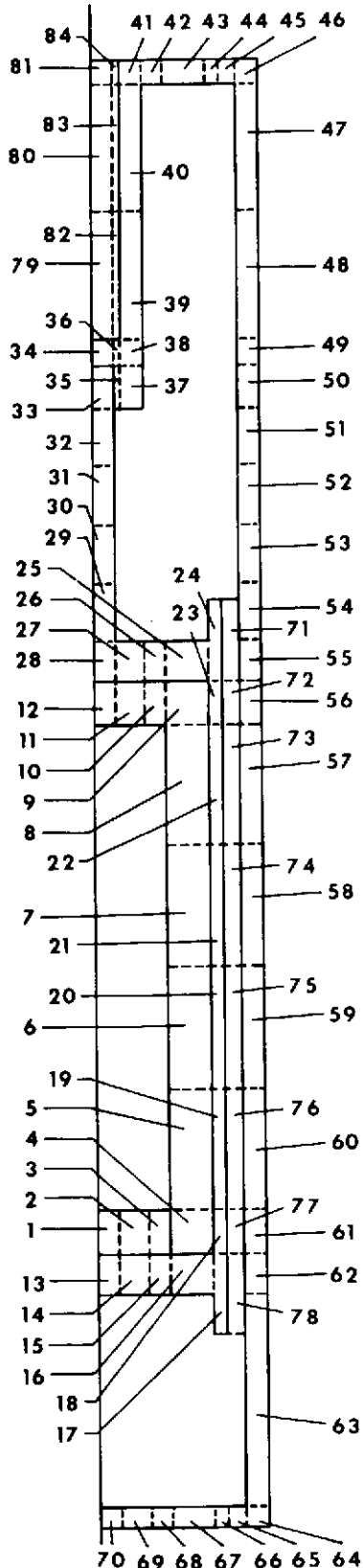


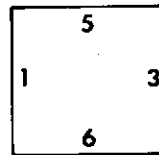
FIGURE 14. THTB NODE STRUCTURE LOWER STEM REGION





Nodes 81, 84, and 41 thru 64 Connected to Water at 135°F with a Surface Coefficient of 1900 Btu/h ft<sup>2</sup> °F

#### 1. Face Numbering Convention



#### 2. Radiation Over-all Exchange Factor Input for THTB

$$F_{12} = \epsilon_1 \epsilon_2 F_{12}$$

Where  $\epsilon_1$  and  $\epsilon_2$  May Be Functions of Temperature

#### 3. Log Weighted $\Delta r$

$$\Delta X_1 = r_i \ln \frac{\bar{r}}{r_i} \quad \Delta X_3 = r_o \ln \frac{r_o}{\bar{r}}$$

#### 4. Face Area

$$A_1 = (\Delta X_5 + \Delta X_6) 2 \pi r_i$$

$$A_1 = (\Delta X_5 + \Delta X_6) 2 \pi r_o$$

FIGURE 16. NODE STRUCTURE USED FOR TΦSS CALCULATION PBR EXP 64-01 R1

TABLE VIII

Typical Temperatures for Nodes of Figures 13, 14, 15 and 16

Node	Temp. (°F)	Node	Temp. (°F)	Node	Temp. (°F)	Node	Temp. (°F)	Node	Temp. (°F)	Node	Temp. (°F)
1	3142.4352	2	3002.4117	3	2972.1745	4	3303.1319	5	3466.3904	6	3537.9003
7	3581.3015	8	3573.6254	9	3519.2102	10	3437.3251	11	3422.5203	12	3418.4994
13	3422.5339	14	3421.0838	15	3421.7709	16	3422.0370	17	3419.5664	18	3389.6936
19	3323.3699	20	3129.2432	21	3553.3017	22	3275.6819	23	2916.0737	24	3007.0250
25	3034.1763	26	3159.1326	27	3185.2306	28	3208.7718	29	3218.8376	30	3220.7102
31	3217.3791	32	3206.7822	33	3180.3065	34	3140.2494	35	3100.8462	36	3014.2994
37	2960.9948	38	2917.8936	39	2895.2009	40	2850.9903	41	2921.8432	42	2951.9507
43	2979.8116	44	3015.9337	45	3044.4190	46	3058.6034	47	3063.3292	48	3060.3694
49	3048.4221	50	3025.3045	51	2989.6169	52	2944.3908	53	2901.3896	54	2866.5245
55	2841.2113	56	2824.0305	57	2797.8401	58	2802.1181	59	2829.9137	60	2843.2418
61	2847.1607	62	2645.7356	63	2514.7660	64	2325.5948	65	2114.3616	66	1899.9260
67	1678.5825	68	1424.7448	69	1379.3016	70	1326.2367	71	1305.0084	72	1243.9975
73	1236.7145	74	1137.6257	75	1135.9372	76	972.2927	77	972.6054	78	773.2768
79	774.8319	80	554.7562	81	556.5997	82	267.5907	83	249.1441	84	161.0329
85	133.3796	86	131.6203	87	131.2799	88	146.8771	89	125.2585	90	1441.8139
91	1467.7752	92	1484.4432	93	1499.7395	94	1513.9132	95	1532.3032	96	1546.9263
97	1554.2617	98	1556.7106	99	1555.1687	100	1548.9907	101	1537.0027	102	1518.6770
103	1496.0265	104	1475.3681	105	1465.2605	106	1516.9815	107	1499.3816	108	130.1982
109	133.8695	110	168.1599	111	188.5273	112	197.1721	113	199.2701	114	200.8869
115	203.2831	116	206.0333	117	208.5529	118	210.3510	119	211.2939	120	211.5396
121	211.1660	122	210.0619	123	207.9585	124	205.4256	125	203.3766	126	200.8262
127	196.4244	128	184.3680	129	155.1501	130	150.7846	131	1212.5465	132	377.8043
133	377.5966	134	2842.3261	135	2847.5821	136	2839.2738	137	2793.4439	138	2729.3021
139	2851.9203	140	2859.1816	141	2844.4572	142	2795.8243	143	2729.2920	144	2852.1066
145	2798.2996	146	2729.3345	147	3392.6717	148	3395.4347	149	3312.1039	150	3164.3499
151	3182.4884										

(GENT-118)

## GEST-2100

properties were considered constant for the TØSS calculations and were a function of temperature for the THTB. There were also some differences in radiation connections and boundary conditions. The difference in calculational results from differences, in the two methods of calculation, result from the difference in nodal structure at the base of the stem.

The following conclusions were made from a thorough review of the diagnostic analyses:

1. Estimated average lower specimen temperatures are  $1662^{\circ}\text{C}$  for No. 3 and  $1621^{\circ}\text{C}$  for No. 4 for the typical data reduced from cycles 41 and 43. These values are close to the target of  $1650^{\circ}\text{C}$  temperature.
2. Estimated average upper specimen temperatures, assuming complete  $\text{UO}_2$  redistribution, are  $1196^{\circ}\text{C}$  for No. 1 and  $914^{\circ}\text{C}$  for No. 2 for the typical data reduced from cycles 41 and 43.
3. The typical fission power generation is 329 watts for the lower specimens.
4. The typical burnup rate for the lower specimens is  $5.5 \times 10^{18}$  fission/cc/cycle.
5. Uncertainties in the knowledge of the operating temperature have been identified. The knowledge of the neutron and gamma flux in the test position and the associated effects on the experiment components continue to be the significant contributors to the temperature uncertainty.

### C. Data Reduction of Experiment 64-01-R1

The operational data was recorded during the testing of Experiment 64-01-R1 for each reactor cycle. This included: nominal reactor power, capsule position in the core, shim rod bank position, temperatures of stem thermocouples of each specimen, the reactor water coolant temperature and total time at power. From these data and gamma heat values for a given shim rod and capsule position supplied by PBRF, the total thermal power, fission power and fuel burnup were calculated.

The stem operating temperatures for each reactor cycle of each specimen are plotted as a function of operating time in Figure 17. As shown in this figure, the temperatures of the lower specimens, No. 3 and 4, parallel each other very closely with only a small temperature difference. The temperatures of the upper specimens, No. 1 and 2, showed a large initial temperature difference relative to the lower specimens and a gradual reduction in the temperature difference during the experiment lifetime. Based on the results of the post-irradiation examination, the large temperature difference between the lower and upper specimens was related to the fuel enrichment which was reversed; i. e., the 2.4% in lower specimens and 1.5% in upper specimens.

The stem temperature to clad temperature calibration was based on complete fuel redistribution. Since the upper specimens had not deposited fuel on the upper end cap, there would be a larger temperature drop between fuel clad and the end cap. Therefore, the fuel and fuel clad of the upper specimens was operating at a higher temperature than predicted from the stem thermocouple temperature reading. The increase in stem thermocouple temperature with irradiation time can then be explained by the  $\text{UO}_2$  fuel redistribution which was occurring in these specimens. The heat transfer gap between the stem end cap and the fuel was decreasing, and hence, a higher temperature was being recorded by the stem thermocouples, and the clad temperature could be constant.

#### D. Post Irradiation Analysis

Post irradiation examination of the capsule consisted of the operations presented in Table IX. The post-irradiation examination was performed in the General Electric Radioactive Materials Laboratory where many of the techniques and procedures used in this examination were established over the years on other fuel irradiation programs and have been proven reliable.

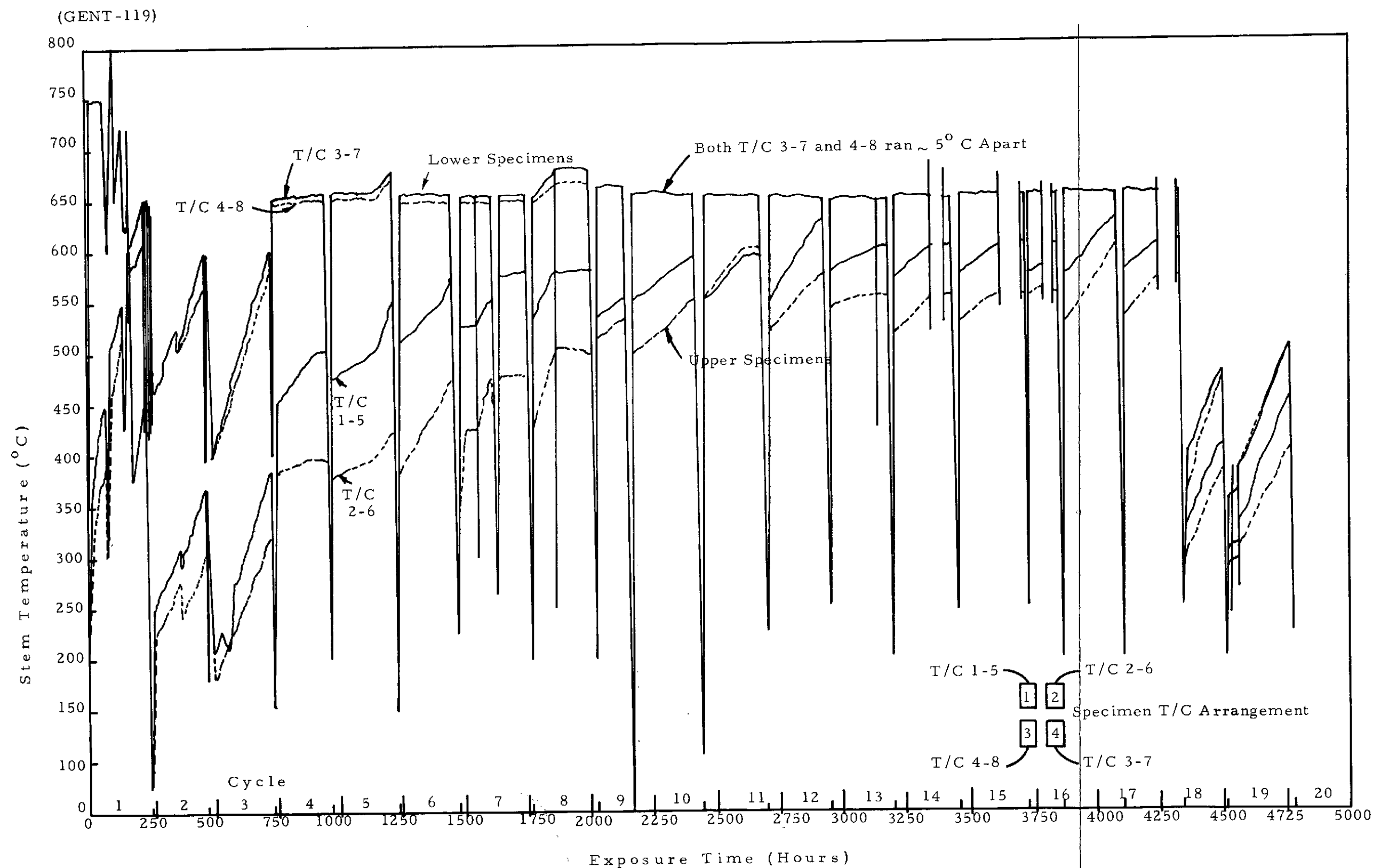


Figure 17. STEM TEMPERATURE PER REACTOR CYCLE FOR EACH SPECIMEN

FOLDOUT FRAME

2

FOLDOUT FRAME /

TABLE IX  
Post Irradiation Operations

Operation No.	Description	Performed on Specimen Nos.			
		#1	#2	#3	#4
1	Analyze Capsule Flux Wires	x	x	x	x
2	Examination of Capsule Holder	x	x	x	x
3	Gross $\gamma$ -Scan of Specimens	x	x	x	x
4	Multi Channel (512) $\gamma$ -Scans of Specimens	x	x	x	x
5	Neutron Radiographs of Specimens		x	x	
6	Thermocouple Calibration			x	
7	Capsule, Gas Analysis by gas Chromato- graphy and Gamma Activity	x	x	x	x
8	Examination and Dimensional Measurements of Emitters	x	x	x	x
9	Perform a Mass Balance of Uranium and Fission Products Inside and Outside of Emitter				x
10	a. Perform a Uranium and Fission Product Plateout Analysis of the Inside of Specimen		x	x	
	b. Perform an Analysis of the Outside Surface of Emitter			x	
11	Perform a Burnup Analysis on the Fuel by Nd, Cs-137 and Heavy Element Measurements		x	x	x
12	Perform an O/U Measurement of the Fuel at od and near Central Void			x	
13	Perform Resistivity Measurements of a W-Re Stem including an Unirradiated Specimen for Reference			x	
14	Metallographic Examinations				
	a. Transverse Cross-Section of Fuel & Cladding		x	x	
	b. Longitudinal Section through a Vent Region- Fuel, Cladding, End Cap		x	x	

## 1. Analysis of Capsule Flux Wires

The portion of the Al-Co flux wire opposite the fuel emitter was removed and analyzed. The four wires were weighed, dissolved, and the Co-60 was recovered and counted. The neutron flux was calculated using an effective thermal cross-section of 42.3 barns and 3340 effective full-power hours. The flux was also calculated based on Nd fuel burnup. A comparison between the calculated neutron fluxes from Co-60 measurements and from Nd measurements is shown in Table X.

TABLE X

Capsule #	Calculated Neutron Flux			
	$\phi t$ (nvt)		$\phi$ (nv)	
	(Nd)	(Al-Co)	(Nd)	(Al-Co)
1	--	$5.6 \times 10^{20}$	--	$4.9 \times 10^{13}$
2	$1.5 \times 10^{21}$	$5.0 \times 10^{20}$	$1.2 \times 10^{14}$	$4.3 \times 10^{13}$
3	$2.4 \times 10^{21}$	$8.8 \times 10^{20}$	$2.0 \times 10^{14}$	$7.6 \times 10^{13}$
4	$2.2 \times 10^{21}$	$7.7 \times 10^{20}$	$1.8 \times 10^{14}$	$6.6 \times 10^{13}$

This comparison shows that the results of flux wires were much lower than that calculated based on burnup. The reason for this difference may be related to shielding of the flux wires by the Inconel sheathed thermocouples which were positioned along the side of the flux wires and the flux perturbation due to the specimen.

## 2. Visual Examination of Capsule

The irradiation capsule upon removal from the NASA/Plum Brook Reactor was clean and essentially free from corrosion or surface deposits. After disassembly of the irradiation capsule at the RML, the four fueled specimens were visually examined and photographed. Localized areas of

bright spots were observed on the surface of the stainless steel containers. The size of these areas was greater for the lower two specimens 3 and 4, which operated at higher power density than the two upper specimens 1 and 2. Only a slight lusterous area was observed on the surface of specimen 1, which according to the operation history had the lowest power density. Based on the emitter dimensions which were measured subsequently, it is believed that these bright spots were associated with areas which operated at a high surface heat flux.

### 3. Gross $\gamma$ -Scan of Specimens

A gross  $\gamma$ -scan was performed on the four specimens prior to dis-assembly. The results of the scans revealed similar  $\gamma$  activity patterns for the companion specimens 1 and 2 and 3 and 4. The  $\gamma$  scans for specimens 2 and 3 are shown in Figures 18 and 19, respectively. These represent a one-to-one dimensional correspondence between the capsule internals and recorded gamma activity record. The two bottom specimens showed a greater activity (note the difference in energy scale between the upper capsule 2 and lower capsule 3), which corresponds to greater number of total fissions. Also, the bottom end of the emitters of each specimen had a greater activity corresponding to the higher neutron flux at the bottom of the emitters. The activity peak at the end of each emitter is related to more  $\text{UO}_2$  at the emitter ends that resulted from  $\text{UO}_2$  redistribution. In the top end of the emitter of specimen 2, the peak was not as high as the lower end of the emitter or as sharp as that of the emitter of specimen 3, which is related to incomplete  $\text{UO}_2$  redistribution in specimen 2.

The large activity spike in the emitter stem of each specimen was associated with the Co-60 activity from the Palco (Pd-Co) braze. An activity peak found on the emitter stem was not expected but subsequent analysis revealed fission product in this region.

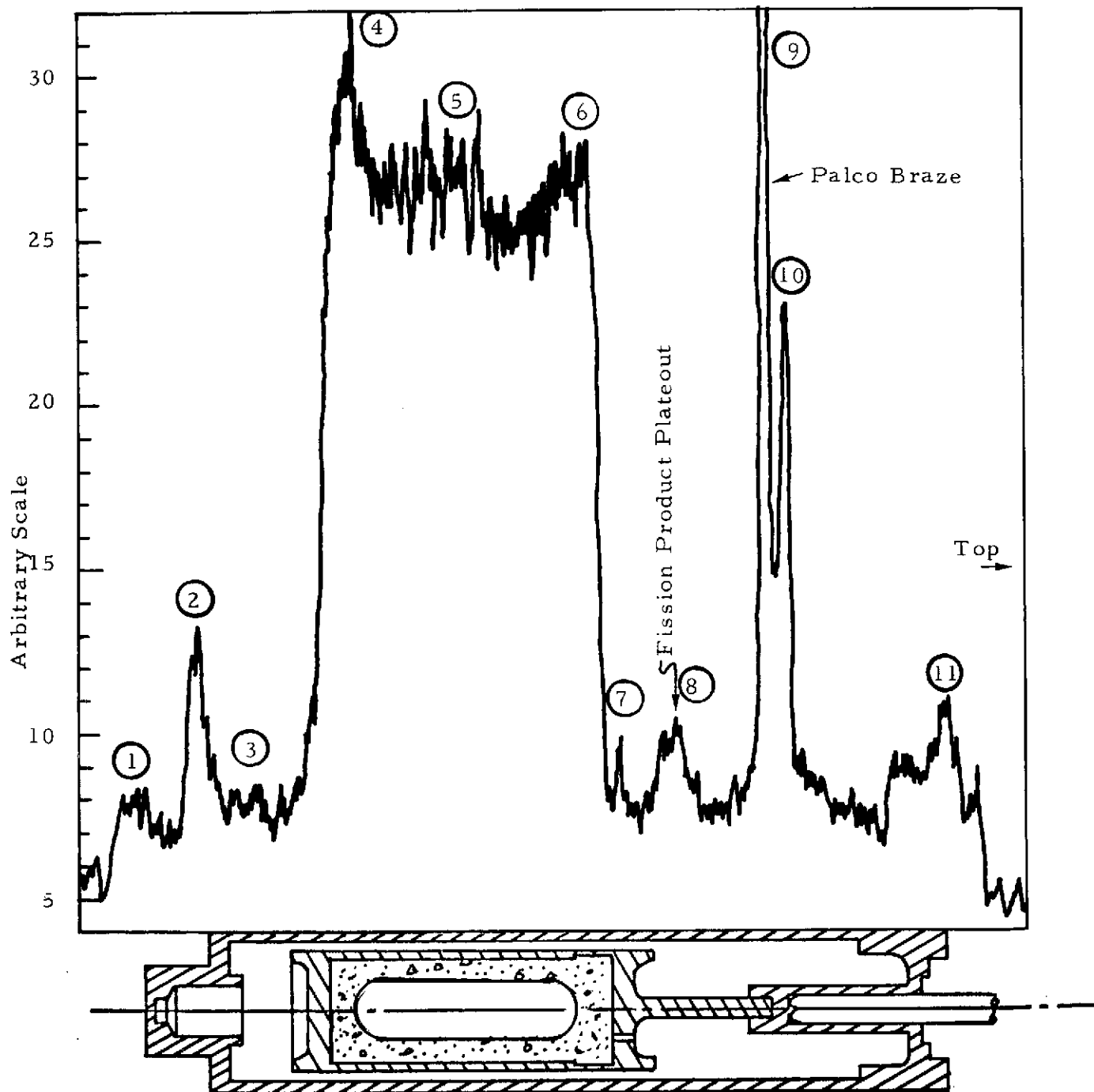


Figure 18. GROSS  $\gamma$ -SCAN OF SPECIMEN No. 2 (THE ONE-TO-ONE CORRESPONDENCE OF GAMMA ACTIVITY WITH CAPSULE INTERNALS IS SHOWN)

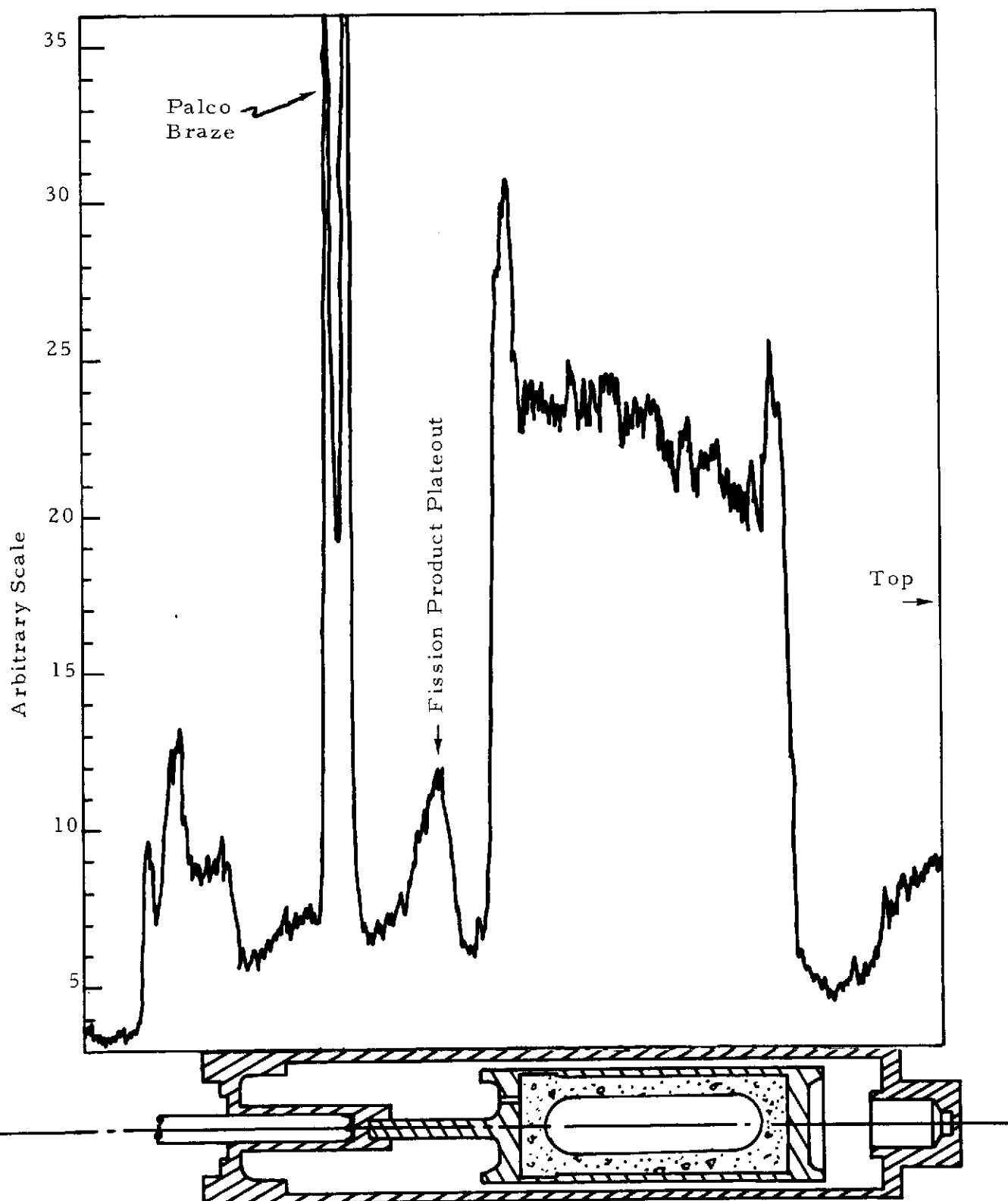


Figure 19. GROSS  $\gamma$ -SCAN OF SPECIMEN No. 3 (THE ONE-TO-ONE CORRESPONDENCE OF GAMMA ACTIVITY WITH CAPSULE INTERNALS IS SHOWN)

#### 4. Multi-Channel (512) $\gamma$ Scans of Specimens

In order to obtain additional information on the fission products and the activity associated with specific areas, 1 through 11 as shown in Figure 18, a 512 channel  $\gamma$  scan was performed on all four emitters. In all four specimens, area 8, the stem region opposite the emitter vent holes, the activity was identified as that resulting from Cs-134 and Cs-137. These products had condensed on the emitter stem. Cs-137 is a volatile fission product, while Cs-134 results from a neutron capture reaction of Cs-133 which is a daughter of Xe-133. In areas 4, 5, and 6, fission products were identified and in the remaining areas, only Co-60 activity was noted.

A second set of 512  $\gamma$  scans was performed on specimens 2 and 4 after the fueled emitter was removed. In specimen 2, which operated at lower power, Cs-134 was detected at the puncture end of the specimen, and Cs-137 and Cs-134 were detected on the emitter stem support region and on the containment can wall opposite the emitter. In specimen 4, which operated at higher power, Cs-134 was detected at the puncture end of the specimen and Cs-137 and Cs-134 were detected on the emitter stem support region, but not on the containment can wall opposite the emitter as in specimen 2.

#### 5. Neutron Radiographs of Specimens

Prior to specimen disassembly, neutron radiography was performed on specimens 2 and 3. The purpose of this examination was to obtain information on gross dimensional changes, fuel redistribution, and other changes of the internals of the specimen so that special care could be taken during disassembly to isolate any failed components.

The neutron radiographs were taken using a collimated beam port in the neutron test reactor. The fueled specimens were placed in front of an iridium plate which was activated and then printed by contact with a film strip. Prints of film of the neutron radiographs of specimens 2 and 3 are

shown in Figure 20. As seen in this figure, complete fuel redistribution had occurred in specimen 3, whereas only partial redistribution had taken place in specimen 2. Also, deformation of the W-25 w/o Re emitter of specimen 3 had occurred while only a slight amount of deformation was evident in the emitter of specimen 2.

#### 6. Calibration of Stem Thermocouples

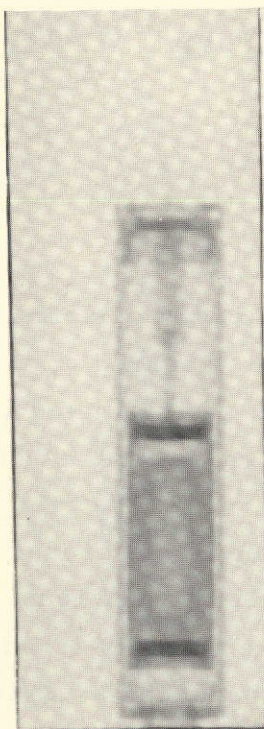
A calibration of the Pt-Pt<sub>87</sub>Rh<sub>13</sub> stem thermocouple was performed in an attempt to determine if a change in emf output had occurred as a result of neutron irradiation. A decrease in emf output of irradiated Pt-Pt<sub>90</sub>Rh<sub>10</sub> thermocouples has been reported<sup>(2)</sup> and occurs as a result of a transmutation of Rh to Pd. This causes a shift in emf toward that of a Pt-Pt<sub>90</sub>Pd<sub>10</sub> thermocouple; a Pt-Pt<sub>90</sub>Pd<sub>10</sub> thermocouple would produce approximately 1/2 the emf of a Pt-Pt<sub>90</sub>Rh<sub>10</sub> couple for any given temperature. Based on this data, it would be expected that the effect of irradiation on the Pt-Pt<sub>90</sub>Rh<sub>10</sub> couples would be to lower the emf produced at a given temperature; i. e., the true temperature would be higher than the indicated temperature. Data on Pt-Pt<sub>90</sub>Rh<sub>10</sub> thermocouples irradiated to a total integrated flux of  $1.8 \times 10^{20}$  at an average temperature of 65°C indicate that for a temperature of 650°C an error of approximately 36°C is introduced. For the stem thermocouples of 64-01-R1, a somewhat greater error would be anticipated because of the greater exposure and slightly different composition.

The thermocouples from capsule 3 were carefully removed from the emitter body and were calibrated against a reference unirradiated thermocouple over the temperature range of 20 to 260°C.

The results of the calibration appeared to be anomalous in that the emf changes were too large, the changes were positive instead of negative and the plot of  $\Delta \text{emf}/\text{emf}$  as a function of temperature was not a straight line. A review of the calibration method using the gradient approach analysis

(GENT-122)

GEST-2100

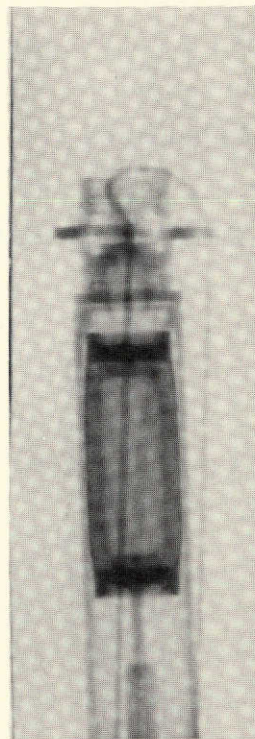


Top

Bottom

Capsule #2

Notice fuel is not completely redeposited.



Capsule #3

Notice fuel is completely redeposited.

Figure 20. NEUTRON RADIOGRAPHS OF SPECIMENS 2 and 3

suggested by Moffat<sup>(3)</sup> did not uncover any information that would invalidate the test data. Furthermore, the unirradiated reference couple provided the correct emf vs temperature relationship. Based on these data, it was believed that an unknown additional source of emf may have been introduced into the irradiated couples which increased with temperature during the calibration. During the irradiation, the thermocouples operated at 650°C; however, the thermocouple calibration was restricted to 260°C because of the limitation of the hot cell calibration device.

Thus, the results of the stem thermocouple calibration appear to be inconclusive. However, if one assumes the reported data and not the results above on irradiated Pt-Pt<sub>90</sub>Rh<sub>10</sub> thermocouples are correct, then the Pt-Pt<sub>87</sub>Rh<sub>13</sub> couples used in the 64-01-R1 would be in error such that the fueled emitters would actually operate at higher temperature than indicated.

## 7. Capsule Gas Analysis

The phase of the RML examination consisted of the collection of the gases within the stainless steel containers of each specimen and an analysis of these gases by gas chromatography and gamma counting for Kr-85. The end cap of each specimen was designed to facilitate an end puncture for the collection of fission gases. This procedure was successful for the recovery of gases from specimens 2, 3 and 4. In puncturing specimen 1, operational difficulties were encountered and the gas sample was lost.

Fission gases Xe and Kr were found in the gas samples from each of the specimens along with helium and argon in a ratio of 1 to 3, which is essentially the ratio used as the filler gas in the specimen and small amounts of nitrogen, oxygen and hydrogen, which were probably air contamination.

Aliquots from each of the three specimens were analyzed for Kr-85 by gamma counting. Those results are presented in Table XI along with

the calculated total number of atoms formed, based on Nd burnup data and the percent release of Kr-85 from the  $\text{UO}_2$  fuel. The release of fission gases from specimens 3 and 4 was very similar and higher than that of specimen 2. These results are consistent with the operating history of the specimens; namely, specimens 3 and 4 were companions which had essentially identical operating histories and which were at higher power densities than specimen 2. The values of fission gas release are also consistent with the results from vented fueled converters operating under similar time, temperatures, and powers under AEC programs.

TABLE XI

Specimen	<u>Kr-85 Gas Release</u>		
	<u>Kr-85 Atoms Released</u>	<u>Kr-85 Atoms* Formed</u>	<u>% Release</u>
2	$3.61 \times 10^{17}$	$4.67 \times 10^{17}$	77.3
3	$8.87 \times 10^{17}$	$10.3 \times 10^{17}$	86.1
4	$8.43 \times 10^{17}$	$9.53 \times 10^{17}$	88.5

\*Based upon Nd burnup measurements

The total Kr-85 gas atoms remaining in the  $\text{UO}_2$  fuel is nearly the same for all three specimens. This indicates that the fuel reaches a saturation value of fission gases.

#### 8. Examination and Dimensional Measurements of the Emitters

The emitters of each capsule were removed by sectioning the capsule at the thermocouple stem end. Specimen 4 which was selected for a determination of a mass balance of fission products and uranium was sectioned with special care in order to minimize contamination of the components.

All of the emitters had very clean surfaces, which were identical in appearance to the pre-irradiated emitters. However, diametral swelling

was evident on all four emitters. Photographs of the emitters of specimens 2 and 3 are shown in Figure 21. Their companions, emitters 1 and 4, were very similar in appearance. In emitters 3 and 4, the surface exhibited a roughened texture which was attributed to the deformation of the emitter. All of the vent holes appeared to be open and free of any  $\text{UO}_2$  plugging or plateout (Figure 21b is typical of all of the emitters).

Dimensional measurements were performed on all the specimens and the emitters. No dimensional changes were detected on the AISI 316 stainless steel containment cans. Measurements on the emitters were made at different axial positions and at two circumferential locations, 0 and  $90^\circ$ . The dimensional changes are summarized in Table XII.

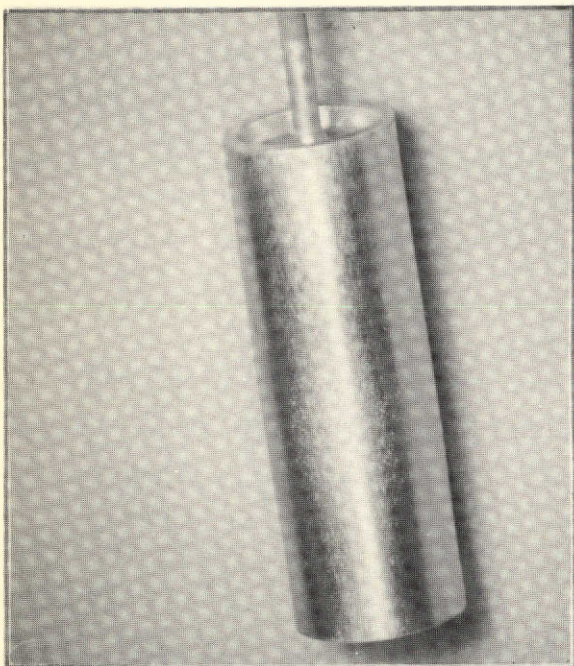
TABLE XII  
Maximum Dimensional Changes in Emitters

<u>Emitter No.</u>	<u>Diametral Changes - inch</u>	<u>Length Changes - inch</u>
1	+0.024	-0.002
2	+0.013	-0.001
3	+0.050	+0.040
4	+0.046	+0.035

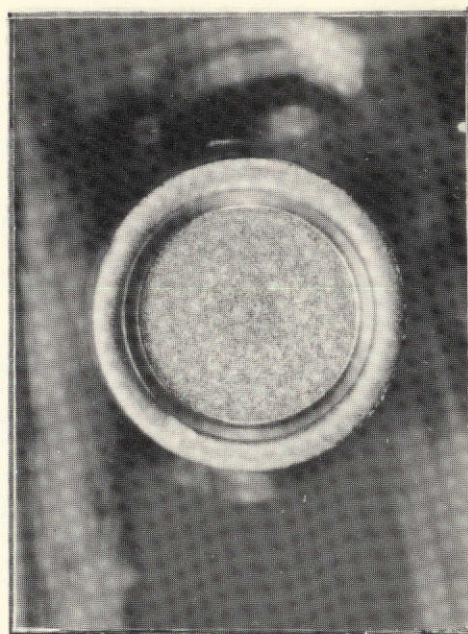
The variation of emitter dimensions as a function of axial position and circumferential locations is shown in the plots of Figure 22. The dimensional changes for the companion emitters, 1 and 2, and 3 and 4, were similar. Also, the amount of deformation was proportional to the emitter power level and the emitter shows more deformation in the region adjacent to the fuel pellet. In the emitters in which complete  $\text{UO}_2$  redistribution occurred, 3 and 4, both diametral and length changes resulted; and in the case of the partially redistributed  $\text{UO}_2$  fuel, emitters 1 and 2, only diametral changes occurred.

(GENT-123)

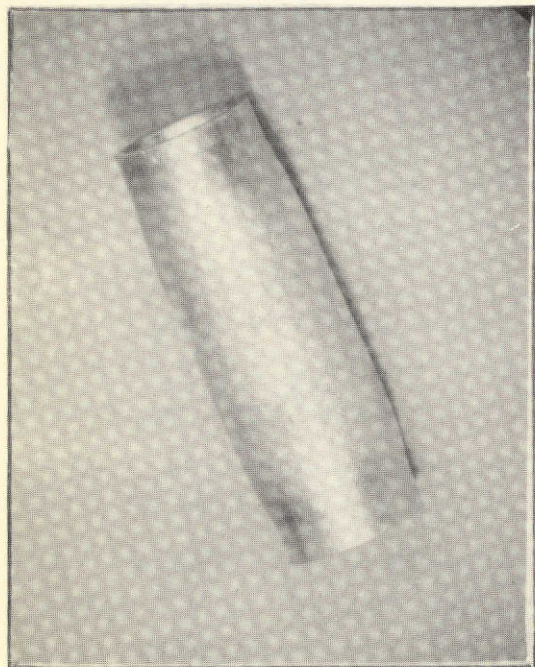
GEST-2100



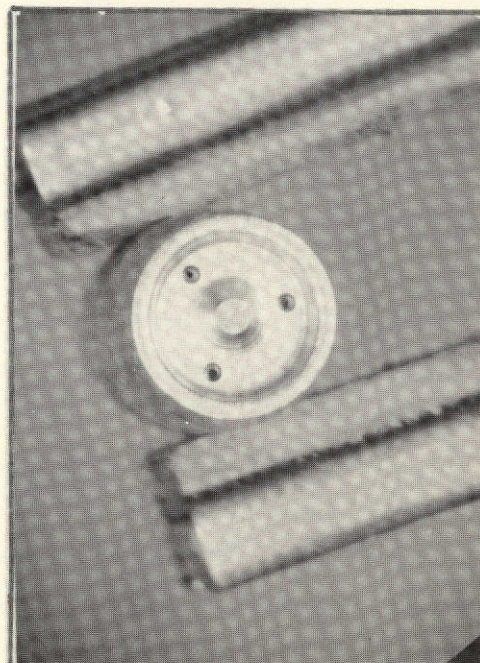
a. Capsule #2 ~2X



Bottom ~3.5X



b. Capsule #3 ~2X



Top Vent Holes ~2X

Figure 21. PHOTOGRAPHS OF W-25 w/o Re EMITTERS  
AFTER IRRADIATION

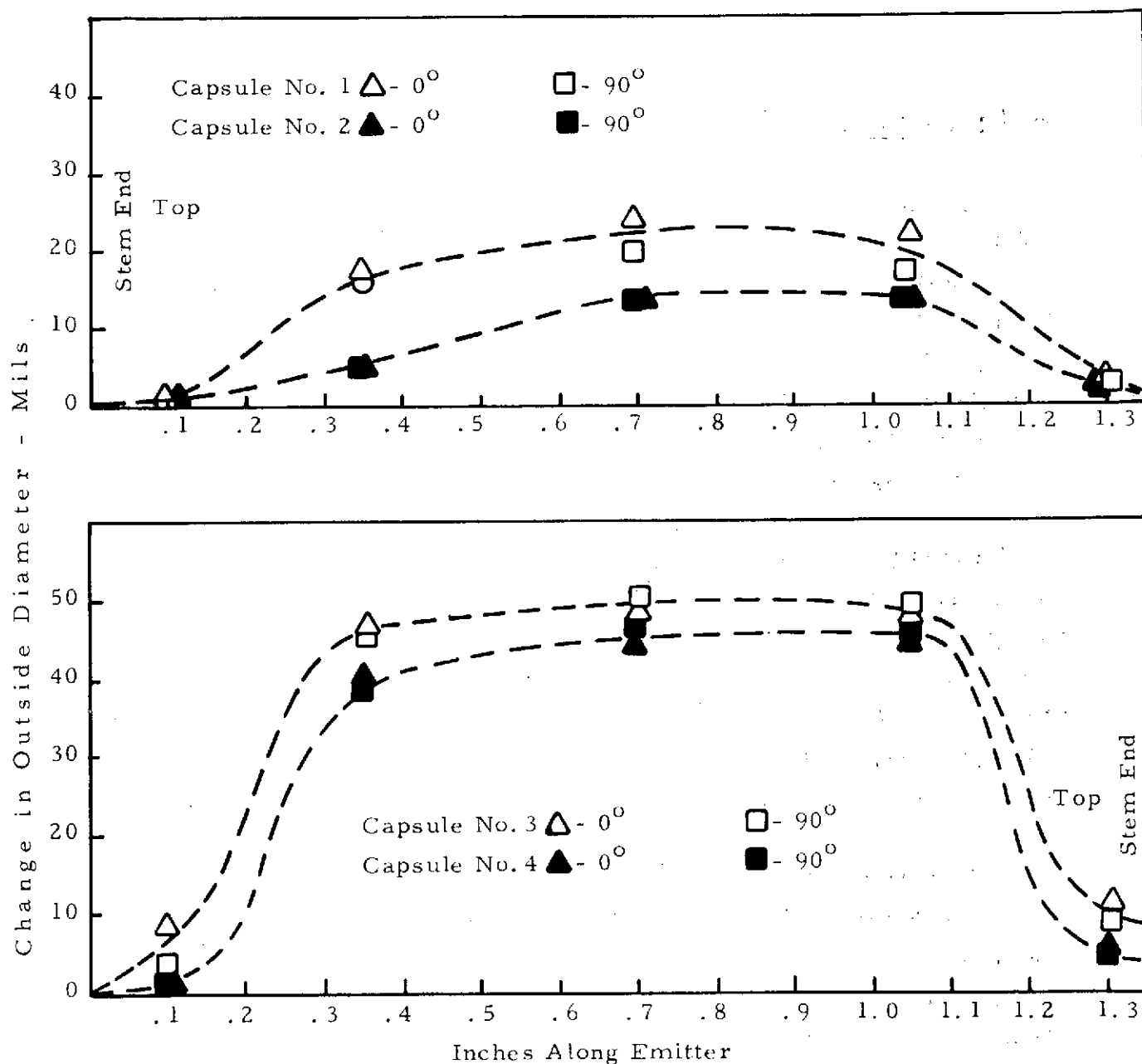


Figure 22. CHANGE IN OUTSIDE DIAMETER OF EMITTERS

## 9. Mass Balance of Fission Products and Uranium

In order to permit the fission gases to escape from the emitter, each of the W-25 w/o Re emitters had three vent holes located on the stem end of the emitter body. The gas analysis of each specimen verified that fission gases had escaped through the vent holes. Since other volatile fission products and  $\text{UO}_2$  fuel could also migrate through these vent holes, it was important to ascertain the extent of fission product movement. Therefore, a mass balance of fission products and uranium was attempted on one of the higher temperature specimens (Specimen 4).

Fission products were recovered from the interior wall of the stainless steel container can, the emitter exterior and stem exterior by an acid solution. The entire fuel sample and the W-25 w/o Re emitter were also dissolved separately. The solutions were analyzed for fission products and uranium. The results indicated that a significant portion of the fission products were lost from the fuel dissolver solution, and therefore, a quantitative mass balance was not possible.

However, the data did yield information on the behavior of fission products. On the interior wall of stainless steel container can, the fission products Cs-137, Sb-125, Zr-95, Ru-103, Ru-106, Ce-141 and Ce-144 were identified. These same fission products were also identified in the solution used to clean the surface of the emitter. In addition, Cs-134 which forms from Cs-133 which results from Xe-133 precursor, was identified along with uranium. In the solution used to dissolve the entire W-25 w/o Re emitter, the only fission products identified were Ru-103 and Ru-106.

The sum total of uranium recovered was within approximately 0.8% of the original uranium minus the portion which fissioned. The total uranium measured outside the emitter corresponded to a calculated  $\text{UO}_2$  weight of 1.94 mgs. This represents a  $\text{UO}_2$  loss rate of 5 mgs/yr or less than 0.03%  $\text{UO}_2$  loss per year per specimen.

With the presence of  $\text{UO}_2$  outside of the emitter, fissioning of the U occurs and contributes to the fission products identified on the capsule wall and surface of the emitter.

#### 10. Fission Product and Uranium Analysis

The interior walls of the 304 stainless steel container of capsules Nos. 2, 3, and 4 were leached to recover the fission products and uranium.

The fission products Cs-137, Sb-125, Zr-95, Ru-103, Ru-106, Ce-141, and Ce-144 were identified in all three capsules. Y-91 was detected only in the solutions of capsules 2 and 4. In all capsules, Cs-134 was found; this specie forms from Cs-133 which is a daughter activity of Xe-133. The amount of the fission products found ranged from  $10^{14}$  to  $10^{15}$  atoms for the refractory elements such as Ru, Zr, and Ce to  $10^{15}$  to  $10^{17}$  atoms for the volatile products such as Cs and Sb.

The fission products detected in the solution from the capsule wall were also identified in the solution recovered from the emitters of capsules 3 and 4. However, Y-91 was not detected in either solution of capsule 3. The number of atoms of the volatile fission products ranged from  $10^{14}$  to  $10^{17}$  while the refractory fission products ranged from  $10^{13}$  to  $10^{15}$ . These were of the same order of magnitude as found in the solution from the capsule wall. The results of the mass balance of fission products in capsule 4 are presented in Table XIII. A quantitative mass balance of the fission products was not achieved because a significant fraction plated out and was lost from the fuel dissolver solution. This also resulted in the poor agreement of calculated total fissions compared to the burnup based upon Nd.

In capsule 4, the total  $\text{UO}_2$  measured outside of the emitter was 1.94 mgs, out of a total fuel mass of 17.7 grams per specimen, which compares to the 2.02 mgs for emitter 3. These results are consistent with the

Table XIII

## Mass Balance of Fission Products and Uranium in Capsule #4

Sample	Atoms							U
	Ce-141	Ce-144	Ru-103	Ru-106	Sb-125	Cs-137	Zr-95	
Leach of Emitter	$9.6 \times 10^{14}$	$2.42 \times 10^{15}$	$<9.0 \times 10^{13}$	$1.18 \times 10^{14}$	$1.91 \times 10^{15}$	$3.60 \times 10^{17}$	$4.53 \times 10^{14}$	$1.46 \times 10^{17}$
Leach of Capsule	$7.41 \times 10^{14}$	$1.88 \times 10^{15}$	$1.28 \times 10^{14}$	$1.34 \times 10^{14}$	$3.08 \times 10^{15}$	$6.98 \times 10^{16}$	$3.33 \times 10^{14}$	$4.19 \times 10^{18}$
Fuel Solution	$1.05 \times 10^{18}$	$1.17 \times 10^{19}$	not detected	not detected	not detected	$8.10 \times 10^{17}$	$2.98 \times 10^{18}$	$3.88 \times 10^2$
Cladding Solution	not detected	not detected	$3.85 \times 10^{16}$	$5.96 \times 10^{16}$	not detected	not detected	not detected	not detected
TOTAL ATOMS	$1.05 \times 10^{18}$	$1.17 \times 10^{19}$	$3.87 \times 10^{16}$	$5.98 \times 10^{16}$	$4.99 \times 10^{15}$	$1.29 \times 10^{18}$	$2.98 \times 10^{18}$	$3.88 \times 10^{22}$
In-Pile Decay Correction	6.29	1.69	5.22	1.80	1.16	1.011	3.45	
Total Atoms Produced	$6.61 \times 10^{18}$	$1.98 \times 10^{19}$	$2.02 \times 10^{17}$	$1.08 \times 10^{17}$	$5.78 \times 10^{15}$	$1.30 \times 10^{18}$	$1.03 \times 10^{19}$	
Effective Fission Yield	0.064	0.0562	0.030	0.038	0.00021	0.0615	0.062	
Fissions	$1.03 \times 10^{20}$	$2.09 \times 10^{20}$	$0.67 \times 10^{19}$	$0.28 \times 10^{19}$	$2.8 \times 10^{19}$	$2.14 \times 10^{19}$	$1.66 \times 10^{20}$	
Fissions (based on Nd burnup)	$3.25 \times 10^{20}$							(total*) $3.91 \times 10^2$

\*Number of U atoms initially present less fission loss

GEST-2100

operation history of the specimens; i. e., companion specimens with near identical operating temperatures.

#### 11. Burnup Analysis of $\text{UO}_2$ Fuel

A burnup analysis of the  $\text{UO}_2$  fuel from specimens 2, 3, and 4 was performed. A ring of the  $\text{UO}_2$  fuel was removed from the center of specimens 2 and 3 and dissolved whereas in specimen 4, all the fuel was dissolved and the burnup was determined on an aliquot of the solution. Nd separations were performed and the resultant Nd concentration was then measured by mass spectrometry. The results of the burnup determinations are presented in Table XIV. The burnup analysis of the fuel from specimen 4 is more accurate than the others since all the fissioning is accounted for in the average burnup obtained by the complete solution of the fuel.

TABLE XIV  
 $\text{UO}_2$  Fuel Burnup Analysis

<u>Fuel From Capsule No.</u>	<u>Burnup in <math>10^{20}</math> Fissions/cc Based on</u>		
	<u>Kr-85</u>	<u>Nd</u>	<u>Heavy Elements</u>
2	>0.73	0.94	0.92
3	>1.78	2.07	2.16
4	>1.70	1.92	1.92

The fuel enrichment requirements for the experiment were 2.5% for the two upper specimens (1 and 2) and 1.5% for the two lower specimens (3 and 4). These enrichments were calculated to provide for equal power generation and to achieve a burnup objective of  $1 \times 10^{20}$  fissions/cc in all four specimens. The results of the burnup data indicated that the enrichments were reversed, and thus account for the difference of a factor of approximately 2 in burnup between the upper (2) and lower (3 and 4) specimens.

12. Measurements of the O/U Ratio of the  $\text{UO}_2$  Fuel

An analysis of the O/U ratio of the fuel from specimen 3 was performed. Fuel samples were removed from the central void region (high temperature region) and from the fuel region adjacent the W-25 Re w/o clad. The O/U ratio was determined by a coulometric technique which was specifically developed for analyzing radioactive samples. The results of the O/U ratio determinations are compared to the pre-irradiation values in Table XV. Within the measurement error there was no change in the O/U ratio with position along the radial temperature gradient of the fuel. Because of the larger uncertainty in the pre-irradiation O/U ratio values, it is difficult to compare the pre and post-irradiation values. The differences in uncertainties in the O/U ratio determinations is related to the refinements in analytical techniques that occurred between the time the fuel was fabricated and the post-irradiation analysis was performed.

TABLE XV  
O/U Ratio Measurements of  $\text{UO}_2$  Fuel  
 Specimen No. 3

	<u>Pre-Irradiation</u>	<u>Post-Irradiation</u>	
		<u>Near Void</u>	<u>Near clad</u>
O/U Ratio	$2.010 \pm 0.010$	$2.002 \pm 0.002$	$2.002 \pm 0.002$

However, the results of the post-irradiation measurements are significant in that the fuel does not exhibit a radial variation in O/U ratio values. Substoichiometry has been reported in  $\text{UO}_2$  at elevated temperatures. (4, 5) Also, with a temperature gradient in the fuel and a vented fuel, there was concern about the loss of oxygen through the vent holes.

Substoichiometry occurs at temperatures above  $1600^{\circ}\text{C}$ , with the degree of substoichiometry dependent upon the actual temperature, time and the environmental conditions. Formation of substoichiometric  $\text{UO}_2$  is accompanied by the precipitation of free uranium upon cooling to low temperatures. The fact that the O/U ratio of the fuel of specimen 3, one of the high temperature capsules, did not show a radial variation indicates that for the times ( $\sim 3400$  hours) and temperature ( $>1650^{\circ}\text{C}$ ) that the O/U ratio did not change with a vented emitter.

### 13. Electrical Resistivity Measurements of W-25 w/o Re Stem

During the in-pile operation of the capsule, there was concern that the thermal conductivity of the W-25 w/o Re stem would change as a function of neutron dose. Therefore, an attempt was made to ascertain the effect of irradiation on the stem thermal conductivity by measuring its electrical resistivity and applying the Wiedmann-Franz Law and the Lorentz relation showing temperature dependency.

The electrical resistivity of the stem from specimen 4 was measured along with an unirradiated control sample. A comparative current-potential method was chosen since this method was believed to yield better accuracy on the small sample (0.075-inch diameter, 0.40-inch long) in the hot cell. The comparative resistivity values had a precision of 1% and the absolute values were accurate to within 8%.

The results of the electrical resistivity measurements are presented in Table XVI.

TABLE XVI  
Electrical Measurements of W-25 w/o Re Stem

<u>Sample and Location</u>	<u>Relative Resistivity .</u>	<u>Resistivity (<math>\mu\Omega</math>-cm) - 100°F</u>
Unirradiated control	1.00	27.3
Irradiated Stem		
Specimen No. 4		
1. Near emitter	1.29	35.2
2. Center	1.21	33.0
3. Near T/C end	1.15	31.4

The differences in electrical resistivity between the unirradiated and irradiated stem may be related to a number of factors, including irradiation damage and compositional variations associated with the formation of sigma ( $\sigma$ ) phase in the irradiated W-25 w/o Re stem. Since a Lorentz number was not available for the W-25 w/o Re alloy, the value used for tungsten was applied to the Wiedmann-Franz Law and the calculated thermal conductivity value for the unirradiated stem fell within a band of the recently published data.<sup>(6)</sup> The value of thermal conductivity used in the original design analysis was obtained in this manner and also was within the band of the measured data.

The variation of resistivity along the irradiated stem may be related to the precipitation of  $\sigma$  phase which would be temperature dependent, and hence, yield an axial variation pattern that parallels the resistivity change. If the change in resistivity was due to irradiation damage, the variation along the stem should have been reversed with the biggest change at the coldest end of the stem and the smallest change at the hot end.

#### 14. Metallographic Examinations

The fueled emitters of specimens 2 and 3 were selected for metallographic examination. These specimens were representative of the lower and higher operating temperatures. Transverse and longitudinal sections of each fueled

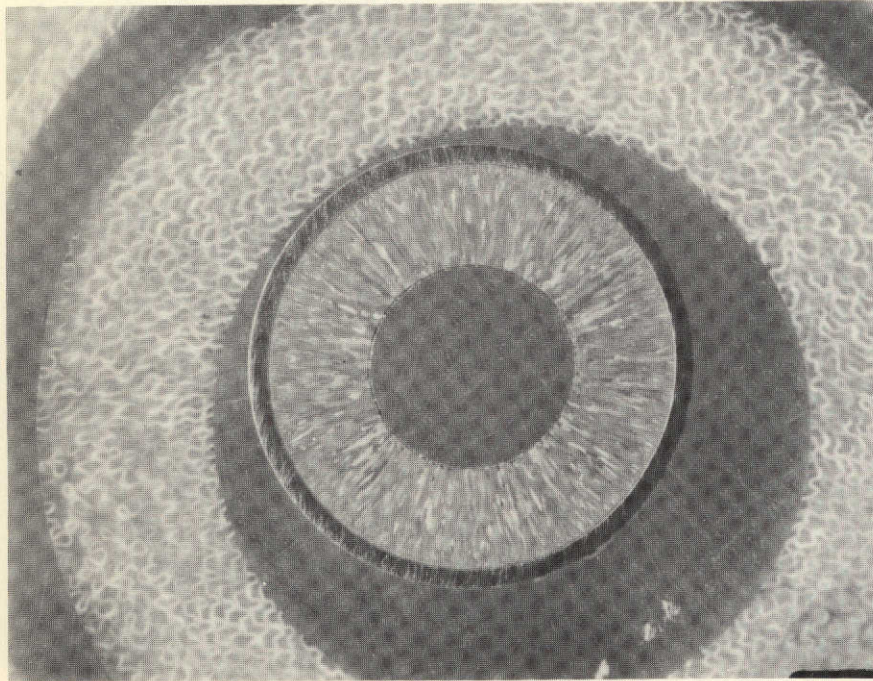
emitter were mounted in epoxy and prepared for metallographic examination. Transverse sections were taken at the emitter midpoint and the longitudinal section was taken through the upper half of the emitter, the vent and stem end.

a. Emitter of Specimen No. 2

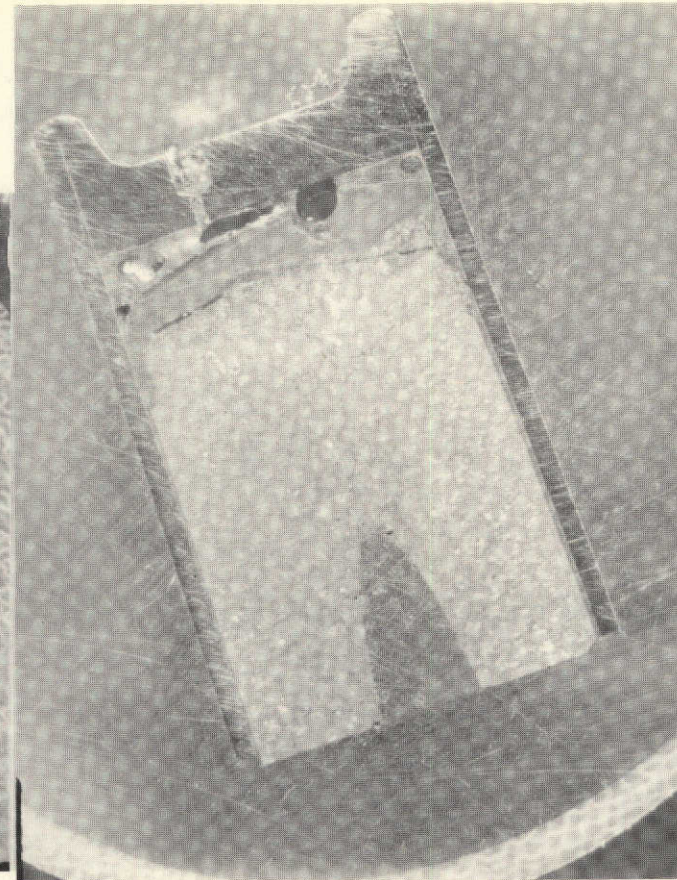
Macrophotographs of the transverse and longitudinal sections of the fueled emitter are illustrated in Figure 23. In the transverse section, large columnar grains were evident in the  $\text{UO}_2$ . This is typical of the  $\text{UO}_2$  that has operated in a thermal gradient at temperatures  $>1600^\circ\text{C}$  for prolonged periods. Observations on the longitudinal section revealed only a partial redistribution of the  $\text{UO}_2$  fuel which is consistent with the results of the neutron radiograph. The vent hole of the emitter is evident in the longitudinal section. In both the transverse and longitudinal sections, the epoxy had filled the gap between the fuel and W-25 w/o Re clad. This gap resulted from the mismatch in thermal coefficient of expansion difference of  $\text{UO}_2$  and W-25 w/o Re. At the operating temperature the  $\text{UO}_2$  was in contact with the clad and upon cool down the  $\text{UO}_2$  pulled away from the clad.

Metallographic observations of the samples revealed a clean W-25 w/o Re- $\text{UO}_2$  interface with no evidence of interaction. These results corroborate the out-of-pile compatibility data.<sup>(1)</sup> The clad- $\text{UO}_2$  interface is illustrated in Figure 24, the montage of the clad and fuel of the transverse section. The W-25 w/o Re clad -  $\text{UO}_2$  cold gap is very obvious in this figure. The  $\text{UO}_2$  fuel was clean with porosity concentrating in the grain boundaries and evidence of lenticular porosity near the central region. Fine spherical metallic particles were evident in the  $\text{UO}_2$ ; these were observed in the starting fuel and are believed to be of a stainless steel composition. Selective etching techniques which dissolve any free uranium verified that these metallic particles were not uranium. One unusual feature of the fuel that was very evident was the high density rim adjacent to the clad. This rim will be discussed in greater detail in the following sections.

(GENT-125)



Transverse Cross-Section ~5X



Longitudinal Cross-Section ~4.5X  
(sample not ground to a full diameter)

Figure 23. TRANSVERSE AND LONGITUDINAL SECTIONS OF EMITTER  
OF SPECIMEN No. 2

CONFIDENTIAL

CONFIDENTIAL

(GENT-126)

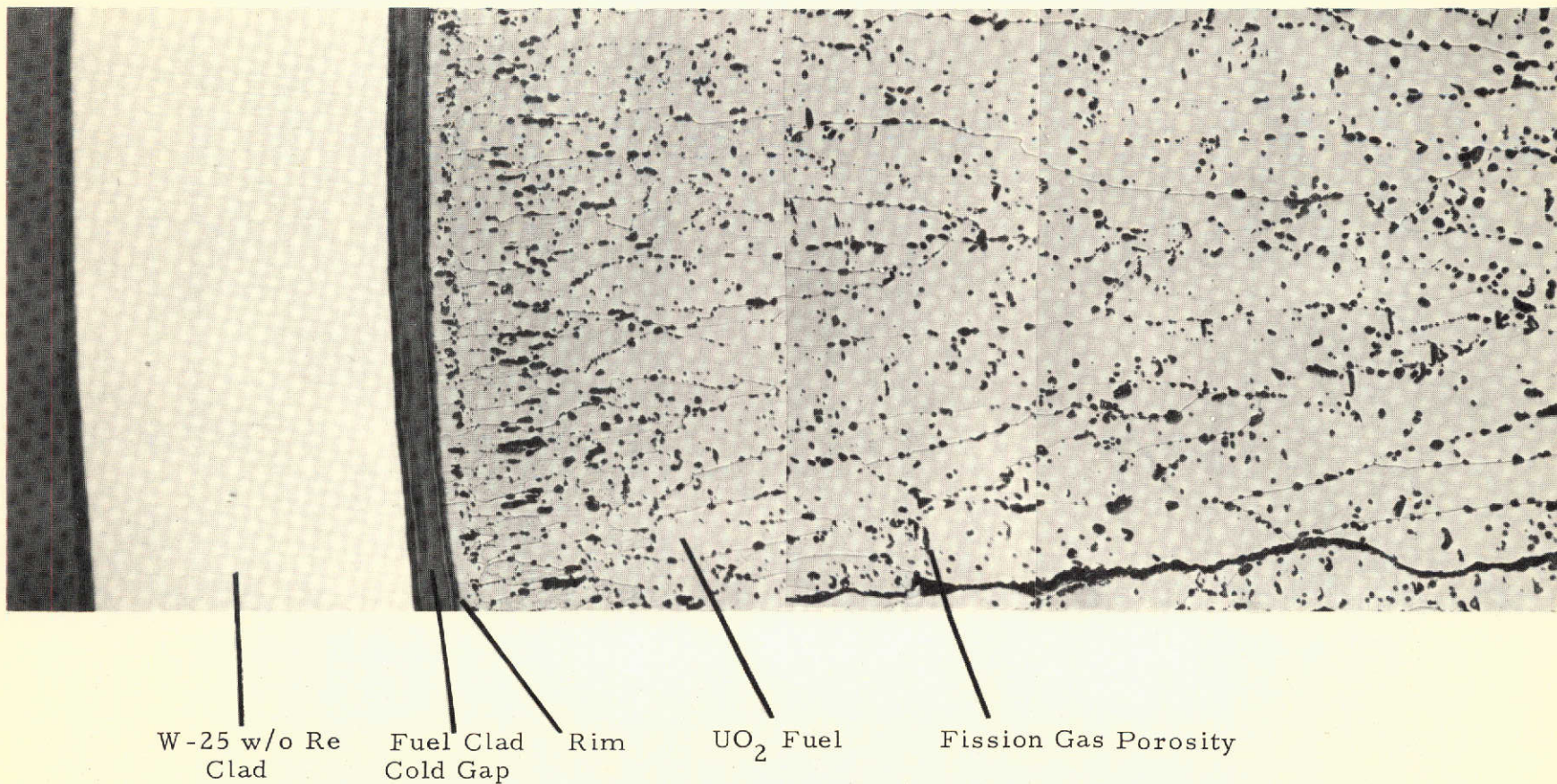


Figure 24. MONTAGE OF W-25 w/o Re CLAD UO<sub>2</sub> FUEL OF TRANSVERSE SECTION OF SPECIMEN No. 2

CONFIDENTIAL

60

GEST-2100

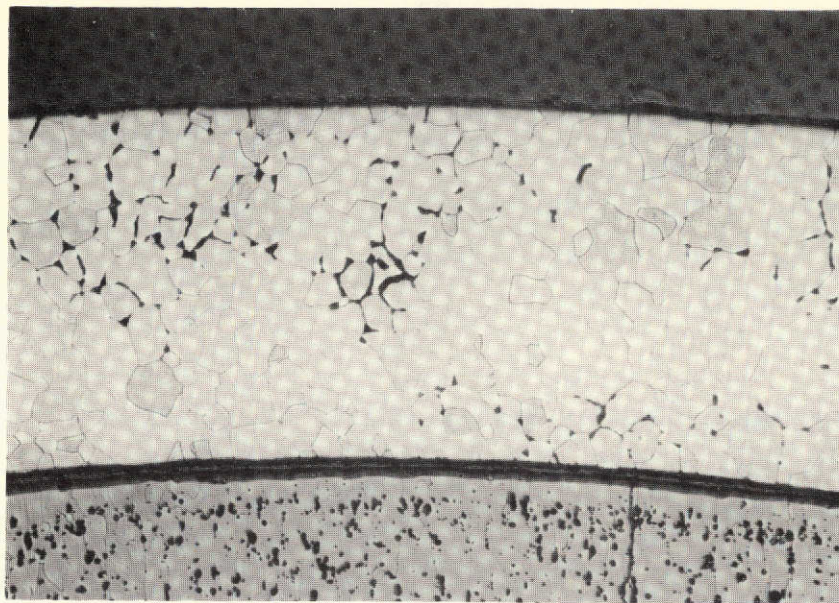
CONFIDENTIAL

In the etched condition, a second phase was evident in the grain boundaries of the W-25 w/o Re clad. This is illustrated in Figure 25, the transverse section of the fueled emitter. As seen in this figure, there was not a complete grain boundary network of the second phase and the grains of the W-25 w/o Re were equiaxed. At high magnifications, an internal structure, spherical in nature, was observed within the grain boundary phase, as shown in Figure 26 at 1000X magnifications. Some of the second phase particles were large enough to permit microhardness measurement; Vickers Hardness Numbers (VHN) as high as 882 were obtained. This indicated that the particles were extremely hard compared to values of 397 VHN of the W-25 w/o Re matrix. This second phase was observed throughout the clad, the weld areas and the end caps. This is illustrated in Figure 27, a photomicrograph of the end cap. Since the end cap was less susceptible to deformation and the fact that the second phase was observed in the end cap to the same degree as the W-25 w/o Re wall, it is believed that the second phase was not strain induced.

In an attempt to explain the presence and the identity of the second phase the W-Re constitution diagram was examined. For the W-25 w/o Re alloy, a single phase solid solution over the operating temperature of the capsule would be predicted from the constitution diagram.<sup>(7)</sup> Sigma ( $\sigma$ ) phase, an intermediate compound forms at rhenium contents of approximately 28 w/o at 1600°C. Because  $\sigma$  is an intermediate compound, it would be very hard. Examination of the as-received W-25 w/o Re material revealed a single phase ( $\sigma$ ) free material. The effects of irradiation<sup>(8)</sup> on many other materials have been studied and while irradiation will affect the kinetics of solid state reactions, it will not alter the phase boundaries of the constitution diagram. Therefore, the irradiation environment likely contributed only to the kinetics of the precipitation of the second phase in the W-25 w/o Re alloy clad.

The effects of the irradiation on transmutation was also considered and for the W-25 w/o Re alloy exposed for 5000 hours in a thermal flux of  $7 \times 10^{13}$  nv plus a similar fast neutron flux component, only causes 0.05 a/o osmium to be formed. This percentage is probably in solid solution and quite

GEST-2100



Etched

100X

Figure 25. SECOND PHASE IN GRAIN BOUNDARIES OF W-25 w/o Re CLAD. TRANSVERSE SECTION, EMITTER No. 2



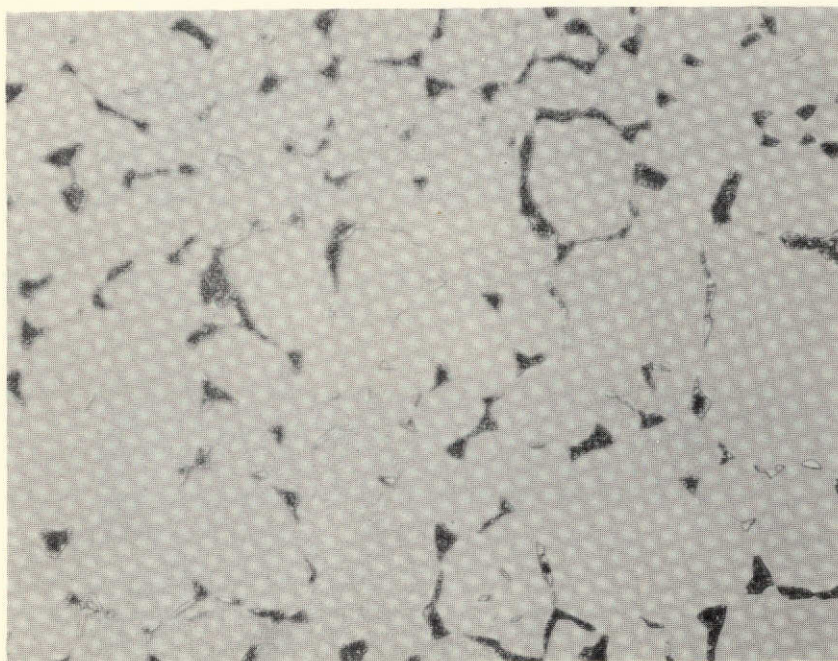
Etched

1000X

Figure 26. SPHERICAL PARTICLES WITHIN GRAIN BOUNDARY PHASE OF W-25 w/o Re CLAD. TRANSVERSE SECTION, EMITTER No. 2

(GENT-128)

GEST-2100



Etched

500X

Figure 27. MICROSTRUCTURE OF END CAP MATERIAL  
OF SPECIMEN No. 2. LONGITUDINAL SECTION

likely was not responsible for the appearance of the large amounts of second phase in the W-25 w/o Re alloys. This phase, based on the hardness values, is probably an intermediate compound and may actually be the  $\sigma$  phase. In discussions with personnel<sup>(9, 10, 11)</sup> of other laboratories, there was general agreement that the phase could be  $\sigma$  and the constitution diagram may be shifted to lower solid solubility of rhenium at the lower temperatures (1600°C and less). Further, they did not know of any work on the W-Re alloys in which homogenization treatments were performed for 3000 hours at temperatures of 1600°C. It is likely that the second phase is  $\sigma$  but further work is necessary to definitely establish the identity of the phase.

One of the three vent holes was examined in the longitudinal section and a photomicrograph of the vent hole for the upper specimen 2 is illustrated in Figure 28. In this figure, a machining burr and two ceramic particles are evident. The two particles were not  $\text{UO}_2$  as determined by alpha autoradiography but are believed to be embedded silicon carbide from the cut-off wheel. The vent hole was free of  $\text{UO}_2$  and completely open.

b. Emitter of Specimen No. 3

The macrophotographs of the transverse and longitudinal cross sections of the fueled emitter of specimen 3 are illustrated in Figure 29. It is evident from these cross sections that complete fuel redistribution had occurred. The wall thickness of the  $\text{UO}_2$  (transverse section) was much less than that of specimen 2 (Figure 23) in which the  $\text{UO}_2$  was only partially redistributed. Columnar grains were also evident in the transverse section and in the vent region of longitudinal section. A cold gap existed between the  $\text{UO}_2$  and the W-25 w/o Re clad.

A montage of the clad and fuel of the transverse section is shown in Figure 30. The microstructures are essentially identical to those observed in the transverse cross section of specimen 2 (Figure 24). There was no evidence of interaction between the clad and fuel. The W-25 w/o Re clad

(GENT-129)

GEST-2100

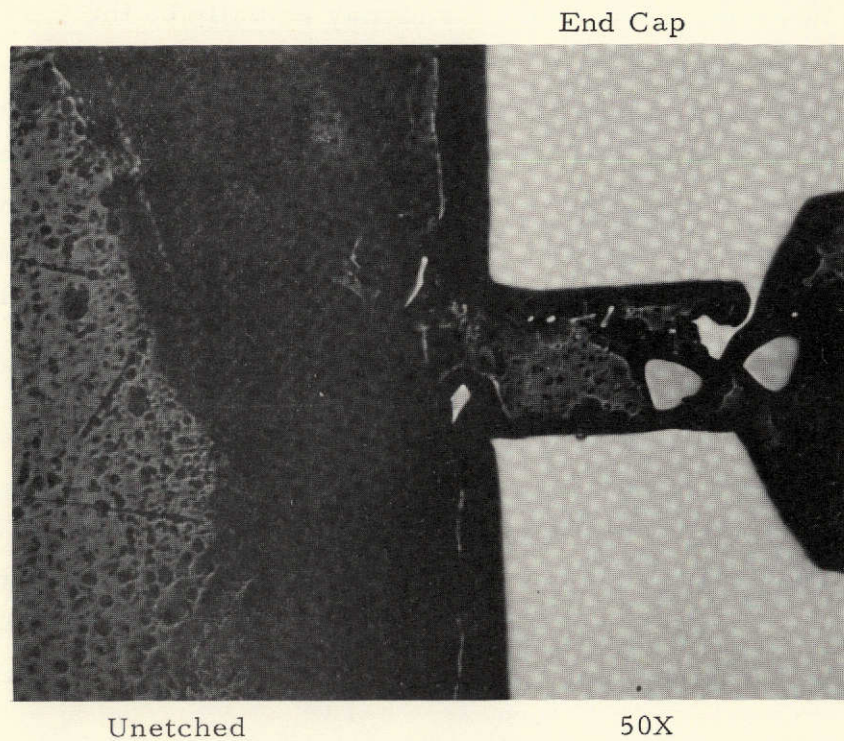
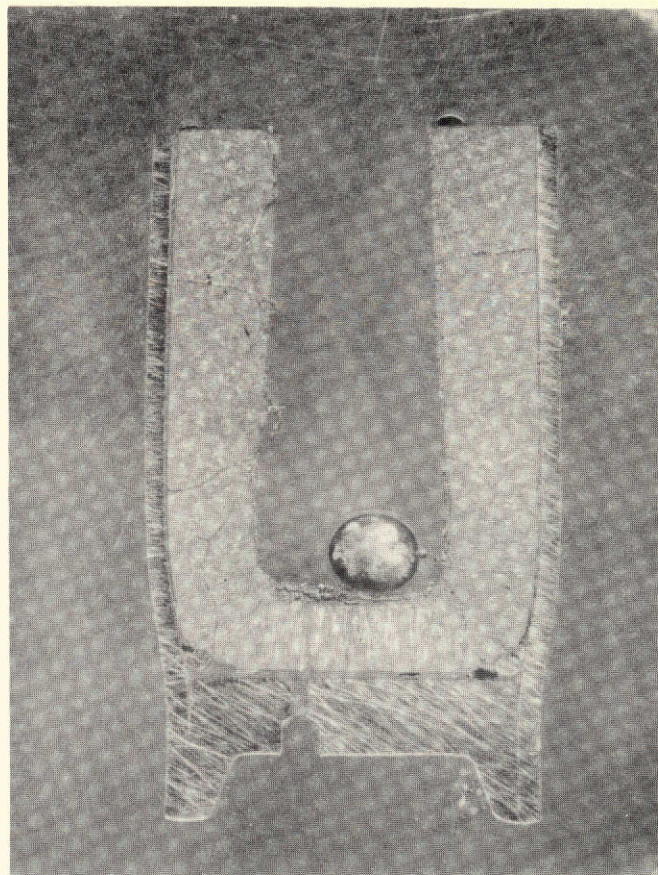
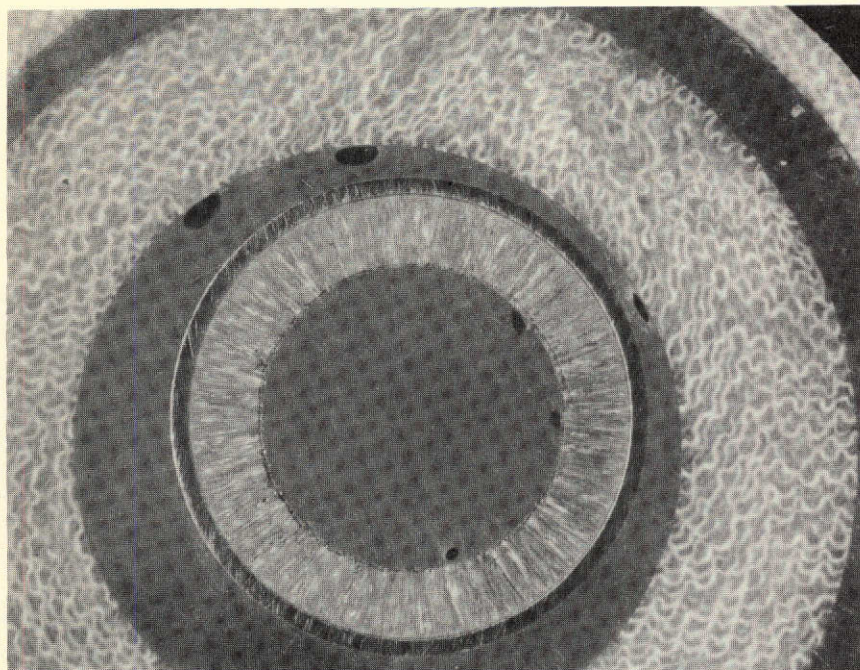


Figure 28. VENT HOLE IN EMITTER OF SPECIMEN  
No. 2. LONGITUDINAL SECTION



Longitudinal Cross-Section ~4.5X



Transverse Cross-Section ~5X

Figure 29. SPECIMEN No.3 TRANSVERSE AND LONGITUDINAL SECTIONS OF THE EMITTER

(GENT-131)

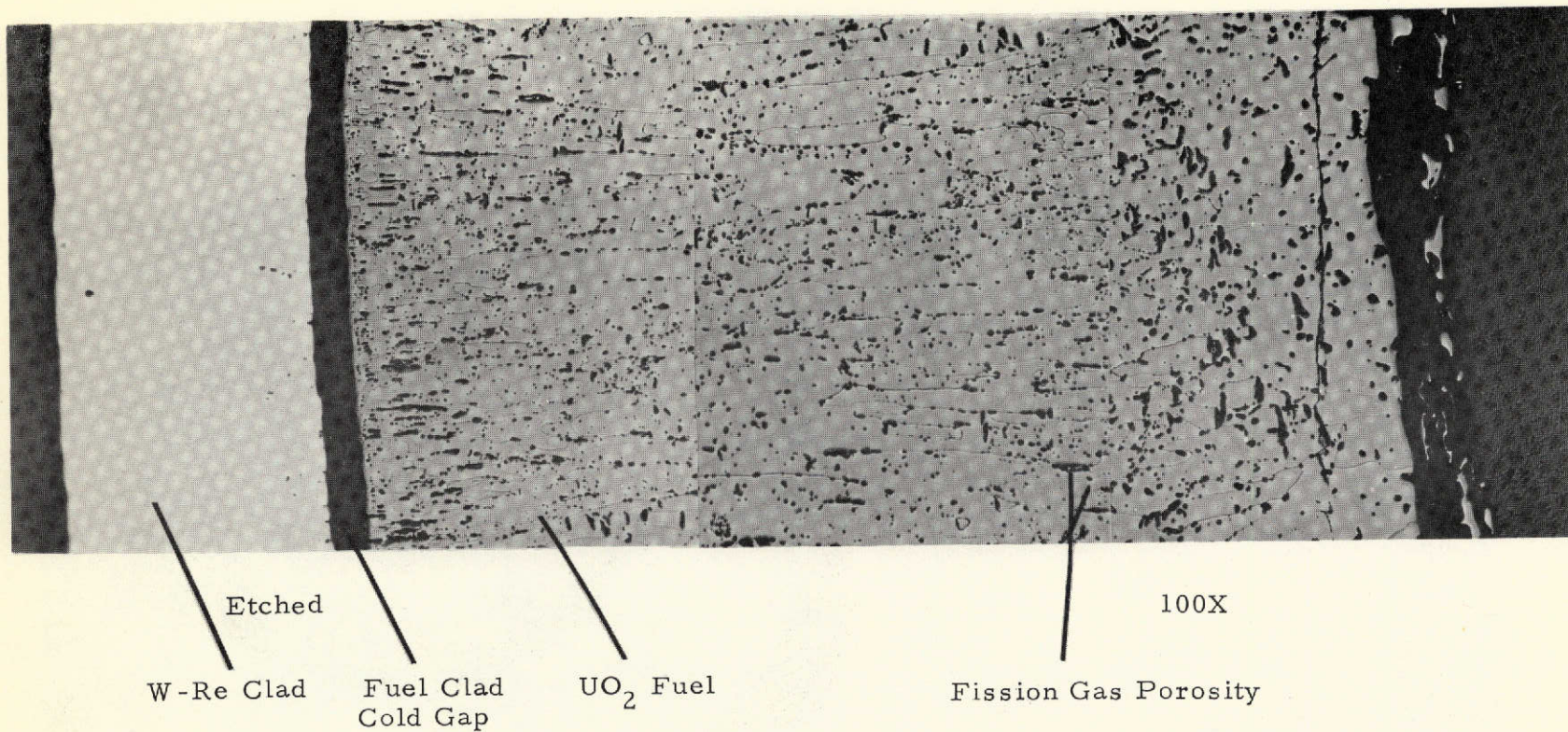


Figure 30. MONTAGE OF W-25 w/o Re CLAD UO<sub>2</sub> FUEL OF TRANSVERSE SECTION OF SPECIMEN No. 3

CONFIDENTIAL

GEST-2100

CONFIDENTIAL

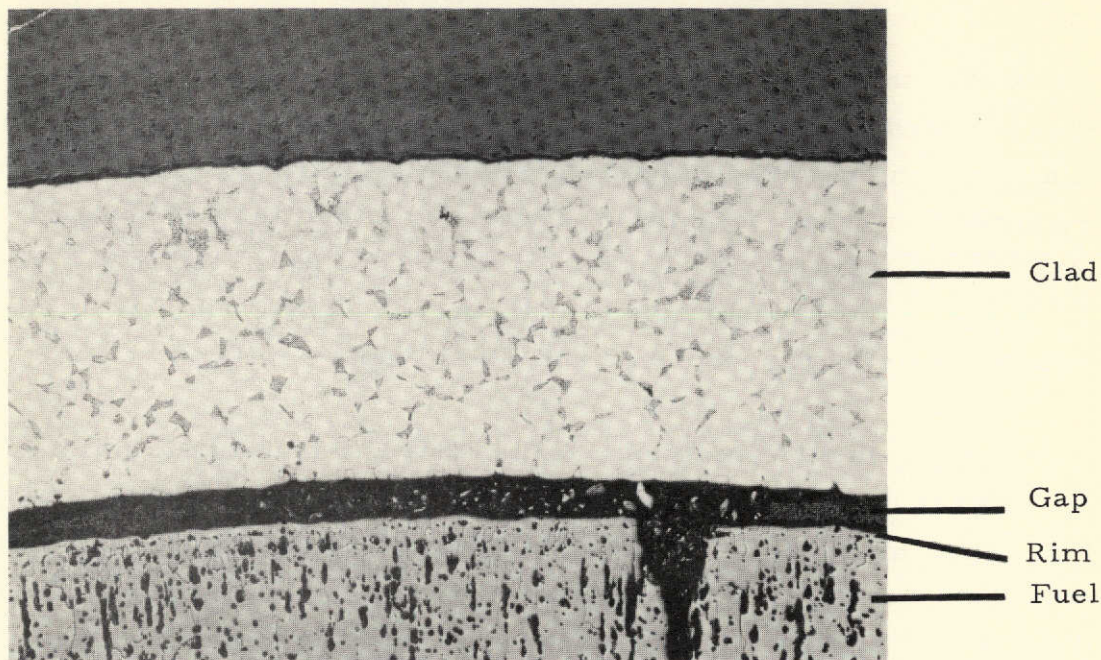
was etched to develop the microstructure. An appreciable amount of second phase located preferentially in the grain boundaries was observed; this is illustrated in the microstructure of Figure 31. The amount of second phase exceeded that observed in the W-25 Re clad of emitter 2 (Figure 25). An internal structure was evident within the second phase and this is clearly discerned in the microstructure of Figure 32. The grain size of the W-25 w/o Re clad of both specimen 2 and 3 were quite similar.

The  $\text{UO}_2$  fuel of specimen 3 exhibited a rim structure similar to that observed in the fuel of specimen 2. However, there appeared to be two rim layers in the fuel of specimen 3 as shown in Figure 31. Observations of the fuel-vent area of the longitudinal cross section of the emitter revealed that the vent passage was not blocked with  $\text{UO}_2$  as shown in Figure 33. The  $\text{UO}_2$  opposite the vent showed a void "pipe" approximately in line with the axis of the vent and it is believed that the formation of the "pipe" may be associated with the mode of  $\text{UO}_2$  evaporation. Alpha autoradiographs of the vent revealed the presence of  $\text{UO}_2$  which is the ceramic phase evident in the vent hole. The second phase in the W-25 w/o Re was also observed in the end cap and weld areas. The  $\text{UO}_2$  shown in Figure 33 also shows evidence of a double rim adjacent to the clad.

The presence of larger amounts of the second phase in the W-25 w/o Re clad of emitter 3 relative to emitter 2 may be related to the higher operating temperature of specimen 3, while a lower temperature would dictate more precipitation from solid solution, the kinetics of the process must also be considered. If for example, the second phase is  $\sigma$ , the precipitation would be favored by higher temperatures since the process is diffusion controlled.

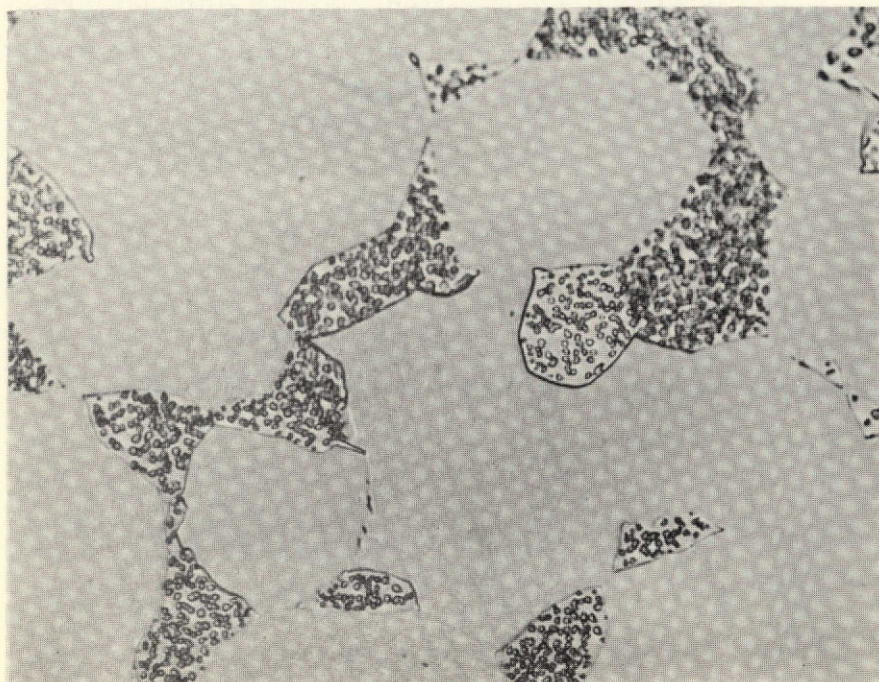
(GENT-132)

GEST-2100

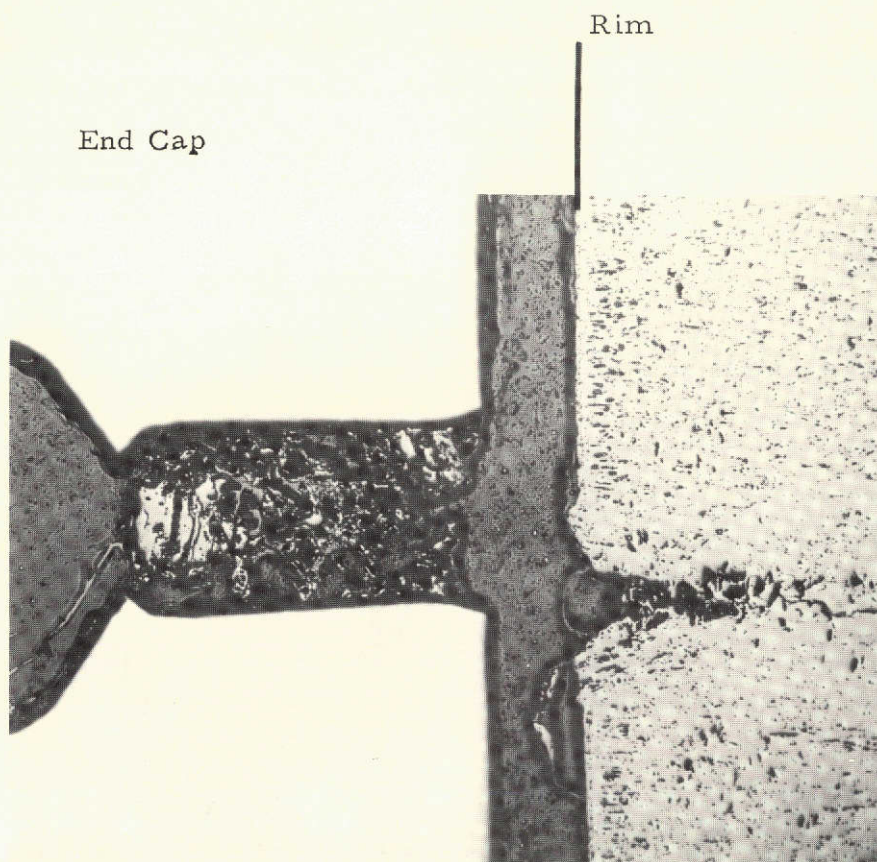


Etched 100X  
Figure 31. SECOND PHASE IN W-25 w/o Re CLAD OF EMITTER No. 3. TRANSVERSE SECTION

(GENT-133)



Etched 1000X  
Figure 32. INTERNAL PHASE WITHIN THE SECOND PHASE IN THE W-25 w/o Re CLAD. EMITTER No. 3, TRANSVERSE SECTION



Unetched

50X

Figure 33. VENT HOLE OF EMITTER No. 3  
LONGITUDINAL SECTION

## E. Proposed Mechanism for Emitter Swelling

A proposed mechanism for the behavior of the emitters was developed after extensive analysis of the operating history and the post-irradiation examination. The logic sequence used in arriving at this mechanism consisted of a review of the post-irradiation observations. These were:

<u>Specimens</u>	<u>Observations</u>
A. 3 and 4 (higher power operation)	1) The $\text{UO}_2$ fuel was completely redistributed. 2) The emitters changed in both diameter and length and the changes ( $\Delta L$ and $\Delta D$ ) were of the same order of magnitude.
B. 2* (lower power operation)	1) The $\text{UO}_2$ fuel was partially redistributed and there was a gap between the fuel and the upper end cap. 2) The emitter changed in diameter only and the amount of deformation was appreciably less than 3 and 4.
C. 2, 3 and 4	1) There was no evidence of chemical reaction between the fuel and W-25 w/o Re clad. 2) A second phase, presumably sigma, was present in the W-25 w/o Re clad with more sigma in the clad of specimen 3 and 4 (higher power). 3) There was no evidence of cracking in the W-25 w/o Re clad. 4) Most of the fission gases (>75%) were released and escaped through the vent hole.

\*Note specimen 1 was not radiographed or examined metallographically.

The deformation of the fueled emitters may be postulated to occur because of several possible interactions. These are: 1) a chemical reaction between the fuel and clad, 2) a mechanical interaction between the fuel and clad, and 3) a combination of chemical and mechanical. The observation that there

was no evidence of chemical reaction between the fuel and clad eliminates items 1 and 3 from further consideration.

The next logical step was to outline the possible modes of mechanical interaction between the fuel and the clad. The interactions that may occur include:

1. Deformation of the cladding resulting from the large mismatch in expansion coefficients during thermal transients (no fuel swelling).
2. Deformation of the cladding resulting from fuel swelling as a function of burnup.
3. Fission gas pressure buildup within the emitter body with resultant deformation of the clad.
4.  $\text{UO}_2$  fuel melting causing large volume change which results in clad deformation.
5. A partial loss of the required fuel/clad gap at intermediate temperatures during both heating and cooling cycles as illustrated schematically in Figure 34. This would result in fuel/clad mechanical interactions with emitter deformation related to the operational history of the test.

(GENT-135)

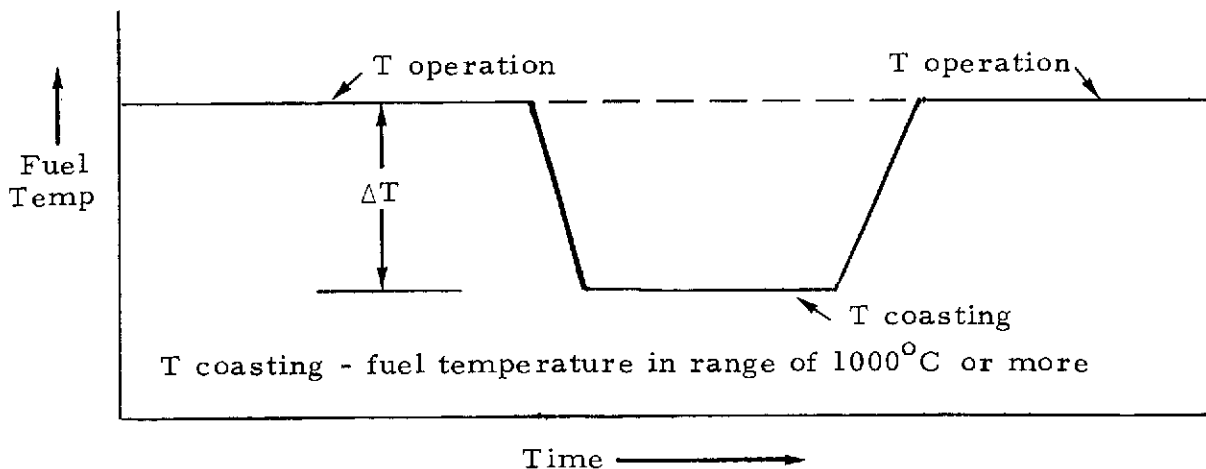


Figure 34. SCHEMATIC FUEL TEMPERATURE CYCLE

## GEST-2100

A rationale based on the operating history and post-irradiation analysis of the 64-01-R1 experiment led to the following reasons for rejection of the first four mechanisms.

<u>Interaction Mechanism</u>	<u>Reason for Rejection</u>
1	In the fuel/clad differential expansion model, large transients yield only small changes in dimensions, significantly less than observed.
2	With approximately 80% of the fission gases released, the fuel swelling caused by residual gases and solid fission products was not sufficient to cause the deformation observed.
3	The emitters were vented and approximately 80% of the fission gases were found outside the emitter. In-pile converters with vented emitters have shown similar fission gas release values and no emitter dimensional changes occurred. Also, a cylinder with internal hydrostatic pressure will expand radially with essentially no change in length.
4	With hollow $\text{UO}_2$ pellets, the calculations indicate that central temperatures of $2800^\circ\text{C}$ were not reached, and there was no operational nor post-irradiation evidence of fuel melting.

The mechanism described in item (5) could not be rejected from the post-test data and it appears that a ratcheting type mechanical fuel/clad interaction is consistent with the observations and operational history. Therefore, an analysis was performed to determine if this mechanism could account for the behavior of the fueled-emitters.

This analysis consisted of the following:

1. A calculation to determine the volume of  $\text{UO}_2$  that would be required to fill a given radial fuel/clad gap.
2. Calculation of the time and temperature required to vapor transport the  $\text{UO}_2$  to fill the gap.
3. A calculation of the trade-off between gap loss due to thermal expansion from heating the fuel and due to the vapor transport of  $\text{UO}_2$  into the gap.

4. A calculation of the gap loss per each cycle of the operating history of the capsule based on the cycles represented in Figure 34 and the comparison of the sum of emitter dimensional changes per cycle with the actual emitter deformation.

This procedure was used in the analysis of one reactor cycle for specimens 3 and 4. The results indicated a possible change of 0.6 mil in the 1 mil available fuel/clad gap associated with the 10-hour cool down from a calculated fuel surface temperature of 2050 to 1530°C. There would also be similar changes in the fuel/clad gap thickness associated with the coasting temperature and heat up to the operating temperature. The reduction in the fuel/clad gap thickness could result in a corresponding increase in emitter dimensions (about 1 mil in diameter) upon heat up to the previous operating temperature. There were 41 thermal cycles involved in the history of the 64-01-R1 experiment and each cycle operating history is similar. Therefore, assuming an average of one mil change in diameter per cycle, this would represent a 41 mil increase in diameter. Also the length for specimens 3 and 4 in which complete fuel redistribution had occurred would increase 41 mil. This compares favorably with the results of specimens 3 and 4 which had increases of 50 and 40 mils in diameter, and 46 and 35 mils in length.

This model, however, has one serious weakness. The transport rates of  $\text{UO}_2$  were calculated for a vacuum environment and not for the actual environment which should suppress the transport rates. However, the presence of Ar-He gas in the gap may cause the  $\text{UO}_2$  to redeposit as a highly porous  $\text{UO}_2$  structure with entrapment of the Ar-He gases in the pores. This Ar-He gas would then be swept into the central void region with the fission gases, vented during shutdown and then recycled during heat up and operation. This porous honeycomb structure could yield the rim observed in the  $\text{UO}_2$  fuel. Since the  $\text{UO}_2$  microstructures represent conditions after operation, it is hypothesized that during operation at test temperatures, the gas voids move up the thermal gradient of the fuel by a process of evaporation and condensation; i. e., pore migration. This

then yields a solid  $\text{UO}_2$  rim followed immediately by a region of pores that have not blended into the normal porosity in the fuel. This hypothesis will be checked by performing an Ar and He gas analysis of the fuel. If measurable quantities of these gases are found in the fuel, this would provide strong evidence in support of the hypothesis and the proposed model for emitter deformation.

## REFERENCES

1. Ekvall, R.A. and Hegland, R.A., NASA CR-72282, "High Temperature Compatibility of  $\text{UO}_2$  with W-25 w/o Re," Topical Report, May, 1967.
2. Ross, C.W., "Effect of Thermal Neutron Irradiation on Thermocouples and Resistance Thermometers," Communications and Electronics, No. 61, P 192-196, July, 1962.
3. Moffat, R. J., "The Gradient Approach to Thermocouple Circuitry," paper presented at the Fourth Symposium on Temperature, Its Measurement and Control in Science and Industry, March 27-31, 1961.
4. Rothwell, J., Nucl. Matl., 6, 229 (1962).
5. Reactor Materials, Fall 1967, Vol. 10, No. 3, USAEC, Division of Tech. Information.
6. GEMP-67. AEC Fuels and Materials Progress Report No. 67, Nuclear Materials and Propulsion Operation, Nuclear Technology Department, G.E., Cincinnati, Ohio, June 30, 1967.
7. Dickinson, J.M. and Richardson, L. S., "The Constitution of Rhenium Tungsten Alloys," Trans. Am. Soc. Metals, 51, 758, (1959).
8. Symposium on the Effects of Radiation on Metals, Nuclear Metallurgy, Vol. III, AIME, 1956.
9. Tarr, C., private communication, G.E. NMPO, Cincinnati, Ohio.
10. Sims, C., private communication, G.E. Matls. and Process Lab., Schenectady, N. Y.
11. Federer, J.I., private communication, ORNL, Oak Ridge, Tenn.

GEST-2100

DISTRIBUTION

Classified Document Control Clerk  
National Aeronautics and Space Administration  
Lewis Research Center  
21000 Brookpark Road  
Cleveland, Ohio 44135

Attention: Roland Brietwieser - M.S. 302-1  
Robert Migra - M.S. 49-2  
James Ward - M.S. 500-309  
Robert Mather - M.S. 500-309  
John E. Dilley - M.S. 500-309  
Report Control - M.S. 5-5  
Technology Utilization Office - M.S. 3-19  
Thomas Moss - M.S. 500-309  
Library - M.S. 3-7  
Neal Saunders - M.S. 105-1  
Robert E. English - M.S. 500-201  
Jack Mondt - M.S. 500-309  
Vincent F. Hlavin - M.S. 3-14

National Aeronautics and Space Administration  
Goddard Space Flight Center  
Greenbelt, Maryland 20771  
Attention: Library  
Joseph Epstein

National Aeronautics and Space Administration  
Langley Research Center  
Langley Field, Virginia 23365  
Attention: Library

Lois M. Robertson, Librarian, M.S. -1L  
Building 4200  
National Aeronautics and Space Administration  
George C. Marshall Space Flight Center  
Huntsville, Alabama 35812

National Aeronautics and Space Administration  
Scientific and Technical Information Facility  
P. O. Box 33  
College Park, Maryland 20740  
Attention: Acquisitions Branch (SQY-34054)

National Aeronautics and Space Administration  
Washington, D. C. 20546  
Attention: Mr. James J. Lynch - Code RNP  
              Mr. Fred Schulman - Code RNP

National Aeronautics and Space Administration  
Lewis Research Center  
Plum Brook Station  
Sandusky, Ohio 44871  
Attention: Henry B. Barkley Jr.  
              Richard F. Barrows

Aerojet-General Corporation  
San Ramon Plant  
P. O. Box 66  
San Ramon, California 94583  
Attention: Sandra Johnson  
              Document Custodian

Aerospace Corporation  
P. O. Box 95085  
Los Angeles, California 90045  
Attention: Library

Air Force Cambridge Research Laboratories  
L. G. Hanscom Field  
Bedford, Massachusetts 01731  
Attention: CRZAP

Air Force Weapons Laboratory  
Kirtland Air Force Base, New Mexico 87117  
Attention: Library

Air Force Aero Propulsion Laboratory  
Flight Vehicle Power Branch  
Wright-Patterson Air Force Base, Ohio 45433  
Attention: A. E. Wallis

National Aeronautics and Space Administration  
Manned Spacecraft Center  
Houston, Texas 77001  
Attention: Library

SAMSO  
Air Force Unit Post Office  
Los Angeles, California 90045  
Attention: Document Control

General Motors Corporation  
Research Laboratories  
12 Mile and Mound Roads  
Warren, Michigan 48090  
Attention: Library

Argonne National Laboratory  
9700 South Cass Avenue  
Argonne, Illinois 60440  
Attention: Library

Atomics International  
8900 DeSoto Avenue  
P. O. Box 309  
Canoga Park, California 91304  
Attention: Robert C. Allen

Babcock & Wilcox Company  
1201 Kemper Street  
P. O. Box 1260  
Lynchburg, Virginia 24501  
Attention: Library

Battelle Memorial Institute  
505 King Avenue  
Columbus, Ohio 43201  
Attention: Don Kizer  
Don Keller

Battelle Memorial Institute  
Pacific Northwest Laboratories  
3000 Stevens Drive  
P. O. Box 999  
Richland, Washington 99352  
Attention: R. F. Dickerson

Bendix Corporation  
Research Laboratories Division  
20800 10-1/2 Mile Road  
Southfield, Michigan 48076  
Attention: Library

Boeing Company  
Aerospace Division  
P. O. Box 3707  
Seattle, Washington 98124  
Attention: Grady Mitcham  
M. S. 22-21

Electro-Optical Systems, Inc.  
300 North Halstead Avenue  
Pasadena, California 91107  
Attention: A. Jensen

Sperry Rand Corporation  
Ford Instrument Division  
31-10 Thomson Avenue  
Long Island City, New York 11101  
Attention: Library

Gulf General Atomic, Inc.  
P. O. Box 1111  
San Diego, California 92112  
Attention: Chief, Technical Infor. Services  
Ling Yang  
M. Simnad  
R. W. Pidd

North American Aviation  
S&ID Division  
12214 Lakewood Boulevard  
Downey, California 90241  
Attention: C. L. Gould

Oak Ridge National Laboratory  
Oak Ridge, Tennessee 37831  
Attention: Library

Office of Naval Research  
Power Branch Code 429  
Department of the Navy  
Washington, D. C. 20360  
Attention: Library

United Aircraft Corporation  
Pratt & Whitney Aircraft Company  
400 Main Street  
East Hartford, Connecticut 06108  
Attention: William Lueckel

Radiation Effects Information Center  
Battelle Memorial Institute  
505 King Avenue  
Columbus, Ohio 43201  
Attention: H. J. Gillette

GEST-2100

Commander, Naval Ships Systems Command  
Department of the Navy  
Washington, D. C. 20360  
Attention: B. B. Rosenbaum

McDonnell-Douglas Corporation  
Douglas Aircraft Division  
3000 Ocean Park Boulevard  
Santa Monica, California 90406  
Attention: A. Delgrossa

The RAND Corporation  
1700 Main Street  
Santa Monica, California 90401  
Attention: Ben Pinkel

TRW Systems  
One Space Park  
Redondo Beach, California 90278  
Attention: Margaret N. Sloane

Thermo Electron Engineering Corp.  
85 First Avenue  
Waltham, Massachusetts 02154  
Attention: George Hatsopoulos  
Robert Howard

Commander J. M. Prosser  
Division of Reactor Development  
and Technology  
Mail Station F-309  
U. S. Atomic Energy Commission  
Washington, D. C. 20545

U. S. Army SRDL  
Fort Monmouth, New Jersey 07703  
Attention: Emil Kittil

U. S. Atomic Energy Commission  
Technical Reports Library  
Washington, D. C. 20545  
Attention: J. M. O'Leary (2 copies)  
D. S. Beard (1 copy)

Institute for Defense Analysis  
400 Army-Navy Drive  
Arlington, Virginia 22202  
Attention: R. C. Hamilton

Radio Corporation of America  
Main Plant  
Electron Component and Devices  
New Holland Avenue  
P. O. Box 1140  
Lancaster, Pennsylvania 17604  
Attention: Library

General Electric Company  
Missile and Space Division  
Valley Forge Space Technology Center  
P. O. Box 8555  
Philadelphia, Pennsylvania 19101  
Attention: Tom Widmer

General Electric Company  
Knolls Atomic Power Laboratory  
1 River Road  
Schenectady, New York 12306  
Attention: R. Ehrlich

General Electric Company  
Nuclear Materials and Propulsion Operation  
P. O. Box 15132  
Cincinnati, Ohio 45215  
Attention: J. W. Stephenson  
for J. W. McGurty  
Report Library

General Electric Company  
Research and Development Center  
1 River Road  
P. O. Box 8  
Schenectady, New York 12301  
Attention: Volney C. Wilson

General Motors Corporation  
P. O. Box 24013  
Indianapolis, Indiana 46224  
Attention: R. R. Blackwell  
Security Coordinator

(NOTE: On inner envelope use above  
address plus: "for delivery to  
T. L. Rosebrock")

GEST-2100

U. S. Atomic Energy Commission  
San Francisco Operations Office  
2111 Bancroft Way  
Berkeley, California 94704  
Attention: C. V. Backlund

Westinghouse Electric Corporation  
Astronuclear Laboratory  
P. O. Box 10864  
Pittsburgh, Pennsylvania 15236  
Attention: Library

University of Arizona  
College of Engineering  
Applied Research Department  
Tucson, Arizona 85702  
Attention: Security Officer  
(NOTE: On inner envelope use  
above address plus: "for delivery  
to Monte V. Davis")

Martin-Nuclear Division  
Martin-Marietta Corporation  
P. O. Box 5042  
Middle River, Maryland 21203  
Attention: W. J. Levedahl

Jet Propulsion Laboratory  
California Institute of Technology  
4800 Oak Grove Drive  
Pasadena, California 91103  
Attention: Peter Rouklove  
Jerry Davis

Lockheed Missile & Space Center  
Technical Information Center  
3251 Hanover Street  
Palo Alto, California 94304 (outer envelope)

H. H. Greenfield  
Lockheed Missiles & Space Center  
1111 Lockheed Way  
P. O. Box 504  
Sunnyvale, California 94086 (inner envelope)

Los Alamos Scientific Laboratory  
P. O. Box 1663  
Los Alamos, New Mexico 87544  
Attention: G. M. Grover  
E. Salmi